National Défense
Defence nationale

ANALYSIS OF THE HF DATA MEASURED AT LEITRIM, USING A MATRIX CALIBRATION METHOD DEVELOPMENT AT DREO (U)

by

Eric K.L. Hung and Zhijiang Hu

DEFENCE RESEARCH ESTABLISHMENT OTTAWA
REPORT NO. 1319

Canada

November 1997
Ottawa

National Défense
Defence nationale

ANALYSIS OF THE HF DATA MEASURED AT LEITRIM, USING A MATRIX CALIBRATION METHOD DEVELOPMENT AT DREO (U)

by

Eric K.L. Hung
Ground Based Group
Surface Radar Section

and

Zhijiang Hu
Telexis Corporation

DEFENCE RESEARCH ESTABLISHMENT OTTAWA
REPORT NO. 1319

PROJECT
05B09

November 1997
Ottawa

ABSTRACT

This is the second report on the analysis of the calibration data taken with a high frequency (HF) antenna array and a signal source towed behind a small aircraft. The analysis described in this report uses the second of two array calibration methods developed by E.K.L. Hung at DREO; the previous report uses the first method. This work is part of a bigger task to develop a calibration method for the HF antenna arrays in the Canadian Forces Supplementary Radio Systems (CFSRS) modernization project.

The calibration method used in this report is superior to the method used in the previous report. The results derived from the calibration data generated with source elevations 31° or lower show that it reduces the deviation of the array beam patterns from the ideal ones, reduces the errors in signal direction estimates, and increases the ability of a high-resolution direction-finding method to resolve signal directions.

RÉSUMÉ

Le présent rapport est le second sur l'analyse des données d'étalonnage recueillies à l'aide d'un réseau d'antennes à haute fréquence (HF) ainsi que d'une source de signaux traînée par un petit avion. Dans ce rapport, l'analyse est réalisée au moyen de la seconde des deux méthodes d'étalonnage du réseau, mis au point par E.K.L. Hung du CRDO; le rapport précédent, quant à lui, traitait de la première de ces méthodes. Cette analyse s'inscrit dans une tâche plus vaste portant sur la mise au point d'une méthode d'étalonnage pour les réseaux d'antennes à haute fréquence dans le cadre du projet de modernisation du Réseau radio supplémentaire des Forces canadiennes (RRSFC).

Dans ce rapport, la méthode d'étalonnage est supérieure à celle que décrit le rapport précédent. Les résultats découlant des données de calibrage, qui proviennent de sources ayant une élévation d'au plus 31°, indique une réduction de la déviation entre les diagrammes de faisceau du réseau et les données idéales, une réduction des erreurs dans les évaluations de direction de signal, et une augmentation de la capacité de la méthode radiogoniométrique à haute résolution qui sert à trouver la direction des signaux.

EXECUTIVE SUMMARY

This report contains a second analysis of the calibration data taken with a high frequency (HF) antenna array in 1994 at Leitrim, near the Ottawa airport. The analysis uses the second antenna array calibration method developed by Eric K.L. Hung at DREO. (The first report is on the analysis of the first method.) It is part of a bigger task to develop a calibration method for the HF antenna arrays in the Canadian Forces Supplementary Radio Systems (CFSRS) modernization project. These arrays are used for detecting long-range HF signals and estimating their directions.

A perfectly calibrated antenna array, in conjunction with a high-resolution direction-finding (HRDF) method, will have the lowest signal-to-noise ratio (SNR) requirement for target detection and the most accurate direction estimates for the array and HRDF method. Calibration errors will raise the minimum SNR required for target detection and reduce the accuracy of the target direction estimates.

The method here calibrates an antenna array through the construction of a calibration matrix for the antenna. It differs from the other matrix methods published in the open literature in that it is tolerant to the presence of interfering signals.

The following observations are based on the analysis of data files generated with signal source elevations 31° or lower:

1. The calibration method reduces the deviation of the antenna beam patterns from the ideal patterns;

2. The method increases the accuracy of direction estimates and suppresses the dependence of errors in bearing estimates on source bearings; and

3. The method increases the ability of a HRDF method to resolve signal directions.

4. The method is superior to the first antenna array calibration method. In particular, the direction estimates are more accurate and

the ability of an HRDF method to resolve signal directions is better.

It is not possible to remark on the results obtained with calibration data generated with signal source elevations higher than 31°. The results are very encouraging. However, these data files have large measurement errors that cannot be suppressed.

TABLE OF CONTENTS

	PAGE
ABSTRACT/RÉSUMÉ	iii
EXECUTIVE SUMMARY	vii
TABLE OF CONTENTS	ix
1.0 INTRODUCTION	1
2.0 HF ANTENNA ARRAY AT LEITRIM	4
3.0 CALIBRATION EXPERIMENTS	7
4.0 DATA PREPROCESSING	14
4.1 Faulty Element Check	15
4.2 Doppler Filtering	18
4.3 File Size Reduction	19
4.4 Correction for Non-Planar Wavefront	20
5.0 CALIBRATION METHOD	22
5.1 Signal Model	22
5.2 Assumptions	23
5.3 Computation of Calibration Matrix	24
6.0 CALIBRATION MATRICES	28
7.0 EVALUATION OF CALIBRATION METHOD	39
7.1 Effect Antenna Beam Patterns	39
7.2 Effect on Direction Estimates	47
7.3 Effect on Resolution of Signal Directions	59
8.0 CONCLUSIONS	67
ACKNOWLEDGEMENTS	68
REFERENCES	69

1.0 INTRODUCTION

The evaluation of an antenna array calibration method [1] developed at DREO is presented here. It uses the calibration data taken in 1994 with a high frequency (HF) antenna array at Leitrim, which is near the Ottawa International Airport. The array received signals from a transmitter towed behind a small aircraft. The objective was to develop a calibration method for the HF antenna arrays in the CFSRS (Canadian Forces Supplementary Radio System) Modernization Project.

High-resolution direction-finding (HRDF) methods are used to process the outputs of HF antenna arrays in the detection of targets and the estimation of their directions. To fully exploit the capabilities of these methods, the arrays must be accurately calibrated. Only in-situ calibration methods can be used, because the arrays are physically very large. Ideally, the methods should account for the mutual coupling among the array elements, the interaction between the elements and local objects, small errors in element positions, and the presence of interfering signals.

An effective way to calibrate an antenna array is to move a signal source over a fine grid of directions covered by the array and measure the array response vectors (array manifold vectors) for these directions. However, this method is impractical, because the computational load in direction finding with these vectors is very high. Besides, different sets of array response vectors are needed for direction finding in differtent environmental conditions (such as wet spring and dry autumn).

The alternative methods treat antenna array calibration as a parameter estimation problem. They note that the outputs of the array elements are usually not ideal and are corrupted by error sources such as unequal element gain and phase responses, mutual coupling among the array elements, and small errors in element positions. These methods calculate a set of calibration coefficients for the array and use them to suppress the errors at the outputs of the array elements.

Many parametric methods for calibrating narrowband antenna arrays have been published in the open literature. They include those by Paulraj and Kailath [2], Friedlander and Weiss [3,4], Brown, McClellan and Holder

[5,6], and Pierre and Kaveh [7], Hung [1,8], See [9,10], and Dogan and Mendel [11]. All methods account for unequal element gains and phases. The method in [8] differs from the others in that it is the only method that can also account for the presence of specular multipath interference. This method has been evaluated by Huang and Hung in [12], using the above calibration data collected at Leitrim. The methods in [1], [4], [7] and [9] and [10] account for mutual coupling and approximate its effect by a matrix operation.

The matrix method in [1] is evaluated here, because it accounts for mutual coupling and preliminary studies indicated that it is also highly tolerant to the presence of interfering signals. The other methods that also account for mutual coupling are ignored here. There are several reasons. Firstly, Hung has shown [13] that the method in [4] sometimes has non-unique solutions. Secondly, the method in [7] produces calibration matrices that are highly dependent on the calibration data. The reasons are given by Hung [1] and See [9]. Thirdly, the methods in [9] and [10] assume the absence of interfering signals. This assumption is usually invalid in the calibration of HF arrays.

The results of this evaluation show that the method in [1] reduces the deviation of array beam patterns from the ideal beam patterns, reduces the errors in direction estimates, and increases the ability of an HRDF method to resolve signal sources close in direction.

In report [12], it was also noted that the method in [8] reduces the errors in direction estimates and increases the ability of an HRDF method to resolve signal directions. When the figures produced by these methods are compared, we note that the method in [1] is superior. In particular, the errors in direction estimates are smaller and do not depend on source bearings. Besides, with the method in [1], the ability of an HRDF method to resolve signal directions is slightly better.

The remainder of this report is organized as follows: Chapter 2 contains a description of the antenna array and the coordinate systems used in the analysis. Chapter 3 describes the calibration measurements and the data collected. Chapter 4 discusses the preprocessing of these calibration data; it includes a check on the possible presence of faulty array elements, Doppler filtering, correction for the deviation of signal wavefronts from spherical wavefronts, and the reduction of the sizes of data files. The matrix calibration method is presented in Chapter 5, and

the calibration matrices it produces are discussed in Chapter 6. In Chapter 7 is an evaluation of the calibration method. It studies the antenna array beam patterns, the accuracy of direction estimates, and the ability of a HFDF method to resolve signal directions. The conclusions are given in Chapter 8.

2.0 ANTENNA ARRAY

The antenna array was located at Leitrim, which is near the Ottawa International Airport. It was planar, had twelve elements, and was part of a larger array with 52 elements. In Table 1 and Figure 1 are the element positions. Given below are the element parameters:

Elements 1 to 8 -

2 inches diameter aluminum pipe, vertical, 20 feet high, antenna feed 7 feet above ground, eight 8-feet ground radials.

Elements 9 to 12 -

2 inches diameter aluminum pipe, vertical, 20 feet high, antenna feed 7 feet above ground, no ground radial.

Elements 9 to 12 were installed in the middle of winter, years after elements 1 to 8.

There are two coordinate systems in Table 1: a UVW-rectangular system supplied with the data and a polar system to be used in the analysis of calibration data. These systems are defined in Figure 2. In the rectangular system, the U-direction is the north direction, the V-direction is west, and the W-direction is up. In the polar system, the location of a point is identified by a triplet (r,θ,ψ). Here, r is the distance of the point from the origin, θ is the bearing angle, and ψ is the elevation angle. The bearing θ is measured in the UV-plane and clockwise from the U-axis.

The rectangular coordinates (u,v,w) and polar coordinates (r,θ,ψ) of a point in space are related to each other by:

$$u = r \cos\psi \cos\theta \ , \tag{2.1}$$

$$v = - r \cos\psi \sin\theta \ , \tag{2.2}$$

$$w = r \sin\psi \ , \tag{2.3}$$

and

$$r = (u^2+v^2+w^2)^{1/2} \ , \tag{2.4}$$

$$\theta = \tan^{-1}(-v/u) \ , \tag{2.5}$$

$$\psi = \tan^{-1}(w/(u^2+v^2)^{1/2}) \ . \tag{2.6}$$

The bearing θ is related to the azimuth angle θ_{az} in an XYZ-coordinate system, defined with {X,Y,Z}={East,North,Up}, by

$$\theta_{az} = 90° - \theta \ . \tag{2.7}$$

The coordinates in the UVW and XYZ systems are related by

$$x = -v \ , \tag{2.8}$$
$$y = u \ , \tag{2.9}$$
$$z = w \ . \tag{2.10}$$

N	ELEMENT POSITIONS					
	Rectangle Coordinate			Polar Coordinate		
	u	v	w	r	θ	ψ
1	3.263	-24.786	0.0	25	82.5	0.0
2	-3.263	-24.786	0.0	25	97.5	0.0
3	-15.219	-19.834	0.0	25	127.5	0.0
4	-19.834	-15.219	0.0	25	142.5	0.0
5	-24.786	3.263	0.0	25	187.5	0.0
6	-19.834	15.219	0.0	25	217.5	0.0
7	23.097	9.567	0.0	25	337.5	0.0
8	24.786	3.263	0.0	25	352.5	0.0
9	85.001	22.776	0.0	88	345.0	0.0
10	-22.776	85.001	0.0	88	255.0	0.0
11	120.741	32.352	0.0	125	345.0	0.0
12	-32.352	120.741	0.0	125	255.0	0.0

Table 1. Element positions in the HF antenna array. Distances u, v, w, and r are measured in meters. Angles θ and ψ are measured in degrees.

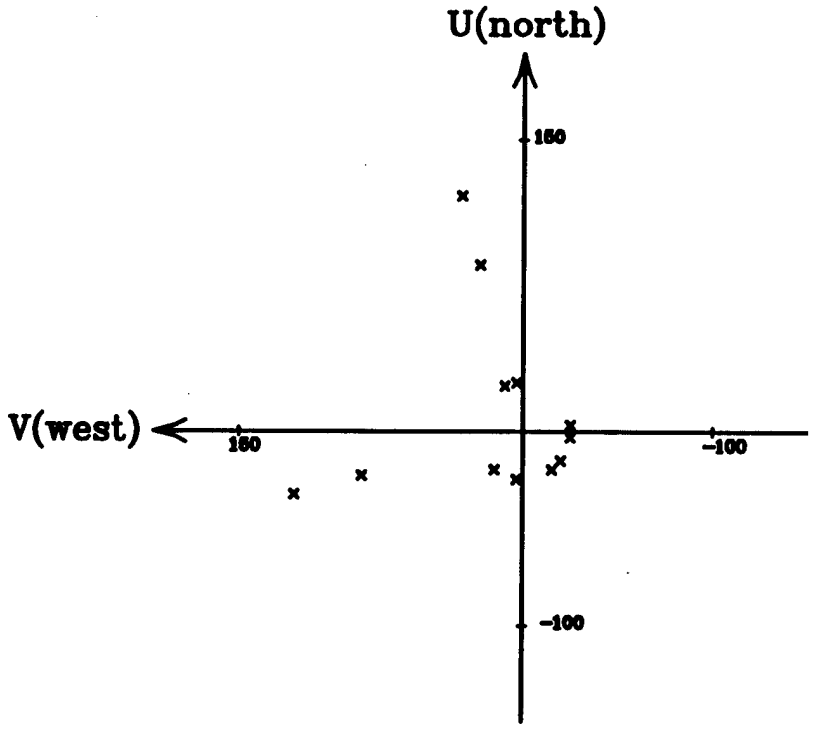

Figure 1. Geometry of Leitrim HF antenna array.

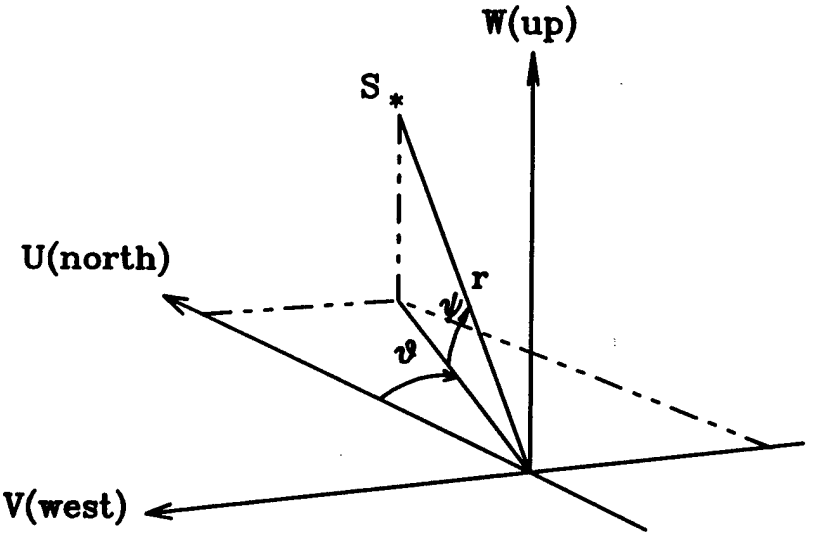

Figure 2. The UVW-rectangular coordinate system and the polar coordinate system.

3.0 CALIBRATION MEASUREMENTS

The calibration data were measured with a vertically oriented dipole transmitter towed behind an airplane. This plane was flown in specified paths while snapshots of the outputs of the array elements were taken. Two global positioning receiver systems were used to determine the ranges and directions of the transmitter in the snapshots. The first, identified as GPS1, was at the antenna site. Its output time, denoted by t1, was recorded with the array snapshots. The second, identified as GPS2, was a differential system consisting of two GPS receivers, one on the plane and the other at a known ground location. Its output time t2 and position $\mathbf{r}_{GPS2}(t2)$ were recorded in a log file on the aircraft at approximately one second intervals.

Six transmitter frequencies were used: 5.1, 7.5, 9.3, 11.5, 15.1, and 18.0 MHz. The outputs at each array element were downshifted in frequency to near-baseband with commonly tuned receivers, sampled with an A/D converter at 10.4k samples/second, and stored in blocks of 8000 array snapshots. Approximately fifty data files were generated.

This study is restricted to the analysis of the data files generated with a transmitter frequency of 5.1 MHz only. In these files, the near-basebands are centred at an intermediate frequency (IF) of approximately 2.0 kHz and the filter bandwidths at the mixers were 3.0 kHz.

Table 2 contains the nominal flight parameters and the sizes of the files at 5.1 MHz. Figures 3 to 10 illustrate the paths of the airplane in these files. They include five clockwise (CW) circles round the array, one counter-clockwise (CCW) circle round the array, and two straight lines over the array.

The flight path in File 2 has a side loop near bearing 210° and a hook near bearing 333°. In this study, we refer to File 2 as the modified file with the side loop and the hook removed.

The transmitter was towed behind the airplane and transmitted a continuous wave signal to the array. Its location at the recorded GPS2 time t2 was approximately the same as that of GPS2 at time t2-Δ, where Δ was equal to the GPS2-to-transmitter distance divided by the speed of

the airplane. The value of Δ was approximately 2 seconds; its exact value depended on the wind speed, wind direction, plane speed, and plane direction at time t2.

In a separate study of the calibration data by Jenkins [14], it was noted that the GPS1 time t1 and the GPS2 time t2, recorded at the same time instant, were related by

$$t2 = t1-\epsilon \ , \tag{3.1}$$

where ϵ was a non-zero difference that was essentially independent of frequency and transmitter elevation. The origin of this non-zero difference was unknown. The study also showed that the transmitter position at time t1, denoted by $\mathbf{r}_{TX}(t1)$, could be derived from the GPS2 position at t2 as

$$\begin{aligned} \mathbf{r}_{TX}(t1) &= \mathbf{r}_{GPS2}(t2-\Delta) \\ &= \mathbf{r}_{GPS2}(t1-\Delta') \ , \end{aligned} \tag{3.2}$$

where $\Delta'=\epsilon+\Delta$. The assignment

$$\Delta' = 8.7 \text{ seconds} \tag{3.3}$$

produced the best overall agreement between the estimated and measured transmitter directions.

File	Date	Planned Track				Data Blocks Recorded
		Elevation (deg)	Altitude (ft)	Radius (km)	Direction	
1	18/05/94	4.5	3000	10	CW	2255
2	20/05/94	11	5000	7	CW	2308
3	20/05/94	11	5000	7	CCW	1438
4	24/05/94	18	6000	5	CW	1106
5	24/05/94	31	6150	3	CW	723
6	24/05/94	49	6000	2	CW	367
7	24/05/94		6000			1350
8	24/05/94		6000			1365

Table 2. Nominal flight parameters for the data files measured at 5.1 MHz. The date format is day/month/year. Each data block contains 8000 array snapshots.

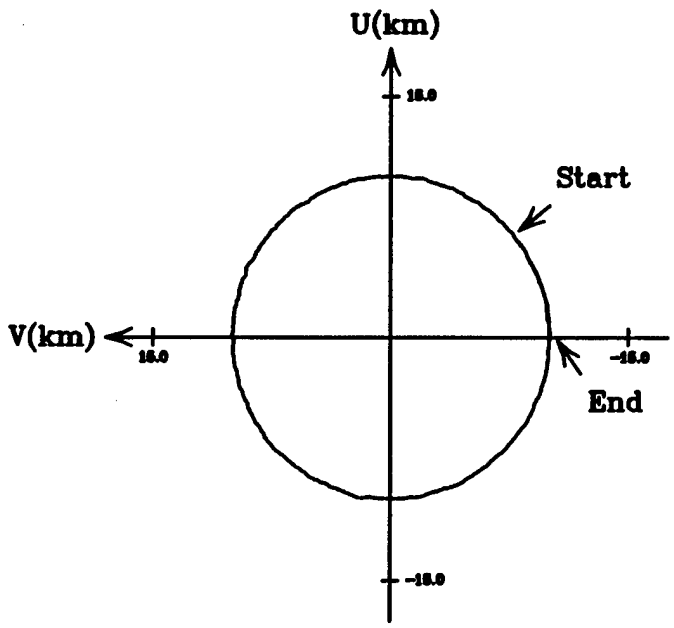

Figure 3. Flight path in File 1. The airplane circles the array with a radius of 10 km and proceeds clockwise (CW) through 405°, from north 45° east to north 90° east.

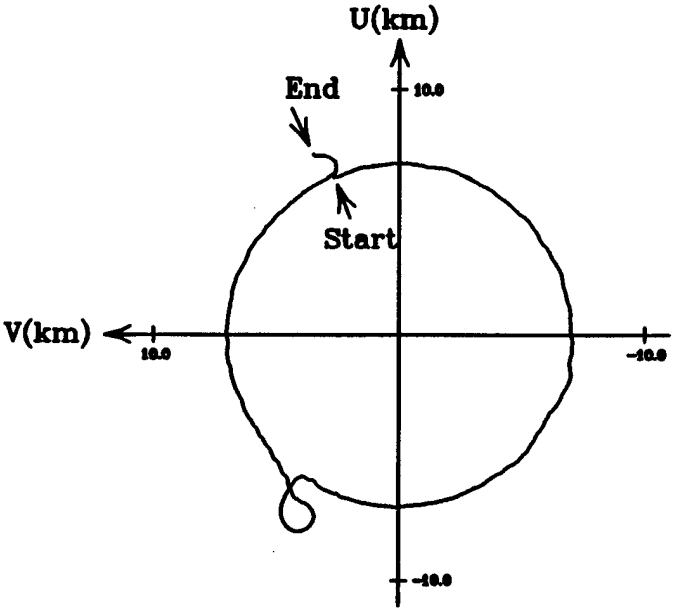

Figure 4. Flight path in File 2 before the removal of the side loop at bearing 210° and hook at bearing at 333°. The airplane circles the array with a radius 7 km, proceeds CW through 358°, from north 24° west to north 26° west.

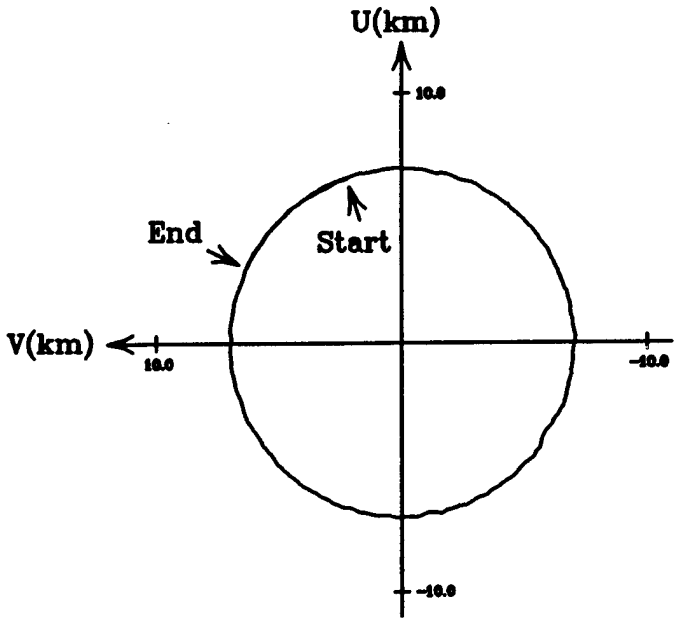

Figure 5. Flight path in File 3: range 7 km; counter-CW (CCW) 405°, north 19° west to north 64° west.

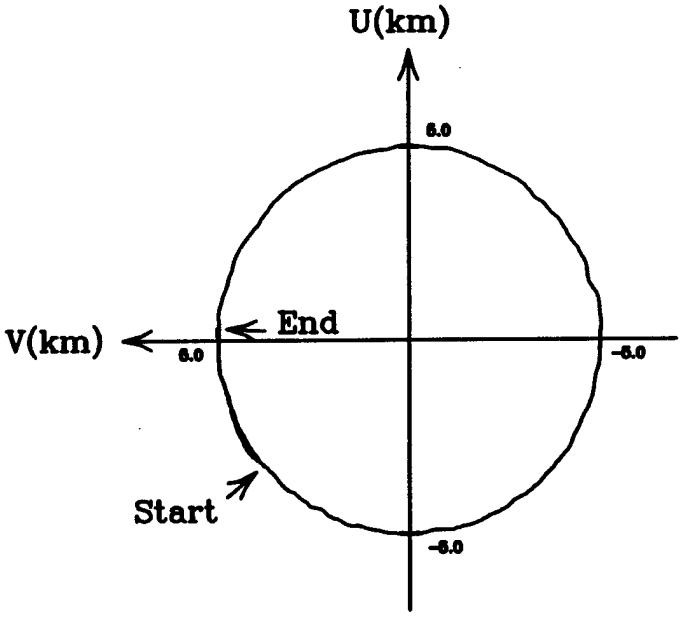

Figure 6. Flight path in File 4: range 5 km; CW 404°, south 49° west to north 57° west.

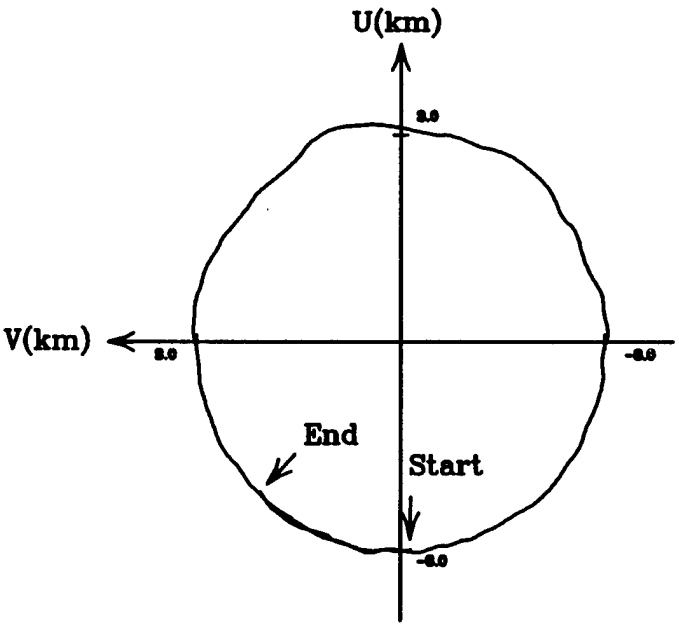

Figure 7. Flight path in File 5: range 3 km; CW 406°, south 3° east to south 43° west.

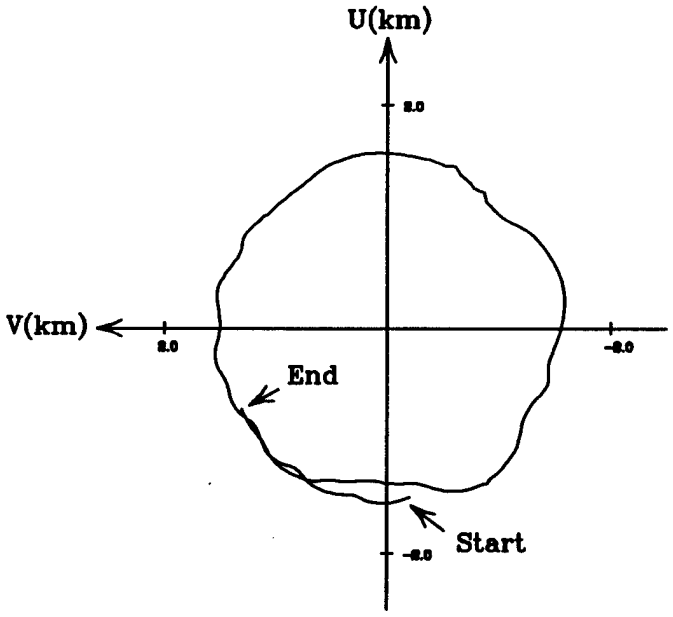

Figure 8. Flight path in File 6: range 1.5 km; CW 429°, south 8° east to south 61° west.

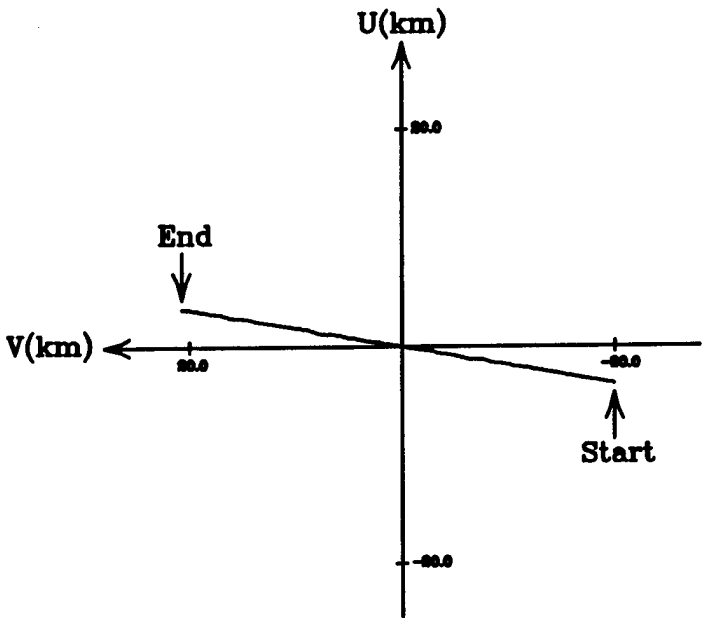

Figure 9. Flight path in File 7. It is a straight line over the array with a heading of west 9.7° north.

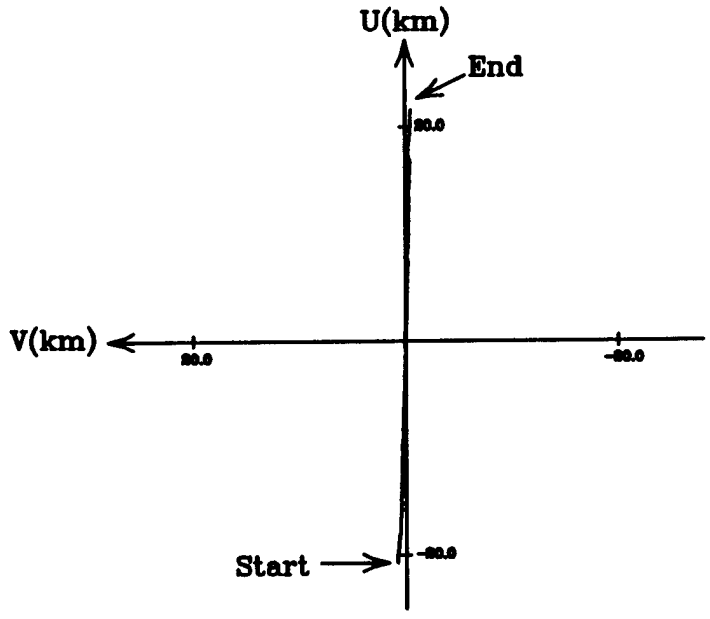

Figure 10. Flight path in File 8. It is a straight line over the array with a heading of north 1.0° east.

4.0 DATA PREPROCESSING

The data files require preprocessing before they can be used to evaluate the calibration method in [1]. This preprocessing comprises the following tasks:

1. Check if there were faulty elements during the experiment;

2. Doppler filter the data in each file to increase the signal-to-noise ratios (SNRs) in the array snapshots by 30 dB and to reduce the number of snapshots in the file by a factor of 1000;

3. Reduce the size of each filtered file further to approximately 3600 snapshots with approximately 0.1° spacing in signal source bearings; and

4. Convert the signal wavefronts in the reduced files to planar wavefronts.

Task 2 is necessary, because the array snapshots in the original files have low SNRs and there are 2.9 to 19 million snapshots per file. Task 4 is also necessary, because the transmitter ranges (track radii) are too short in the files.

There are two measurement errors that cannot be corrected in the preprocessing. The first is intrinsic to the antenna array and originated from the misalignment of the array elements. It has been assumed that the aluminum pipes used in the array elements were vertical and, therefore, parallel. The relative orientations of some pipes were checked with the parallax method in the summer of 1995. They were not exactly parallel, as the angle between two pipes was several degrees in some cases. This misalignment perturbed the gain and phase responses of the array elements. The perturbation increased with transmitter elevations and varied slowly with the transmitter bearing. The second error is an artifact that originated from the short transmitter ranges in data generation. These ranges were 10 km or less. Consequently, one cannot ignore the difference in the transmitter elevations at the array elements. This error also perturbed the gain and phase responses of the elements. Usually, the perturbation was larger if the transmitter range

was shorter.

File 6 in Table 2 was measured with a rather high transmitter elevation of 49° and a rather short transmitter range of 2.0 km. The measurement errors due to the above perturbations are so large that this file is not expected to produce reliable results in the study. Files 7 and 8 have too many snapshots measured with transmitter ranges shorter than 2 km and elevations higher than 49°. They are not used in this study.

4.1 Faulty Element Check

By design, the transmitter signal at the array elements was very strong compared with the other signals. The frequency of this signal in the data files is close to the IF (≈2.0 kHz) at the receivers, because the nominal transmitter range was constant and the corresponding Doppler frequency of the transmitter was zero. Therefore, the antenna array was unlikely to have faulty elements if (a) the spectrum of the outputs of each element has a very strong signal present, (b) the frequency of this signal is the same for all elements, and (c) this frequency is close to 2.0 kHz.

Some results obtained in a check for faulty elements are presented in Figs. 11 and 12. They were produced with the Fast Fourier Transform (FFT) and the first 1000 array snapshots in the first block of Files 1 and 2, respectively. Each figure has twelve spectra, one from the outputs of each array element. Because the figures are crowded and the spectra in the same figure look alike, the element identification numbers have been omitted. A separate study shows that, in each spectrum, the strongest amplitude has a frequency of 1.95 kHz and is at least 25 dB stronger than the other signals. Therefore, the array was unlikely to have faulty elements during the generation of Files 1 and 2.

Three identifiable interfering signals are present in the spectra. Their frequencies are 0.00, 0.06 and 3.08 kHz. The 0.00 Hz signal probably came from offsets in the A/D converters. The origins of the others are unknown.

Similar studies showed that the antenna array was also unlikely to have faulty elements during the generation of Files 3 to 6.

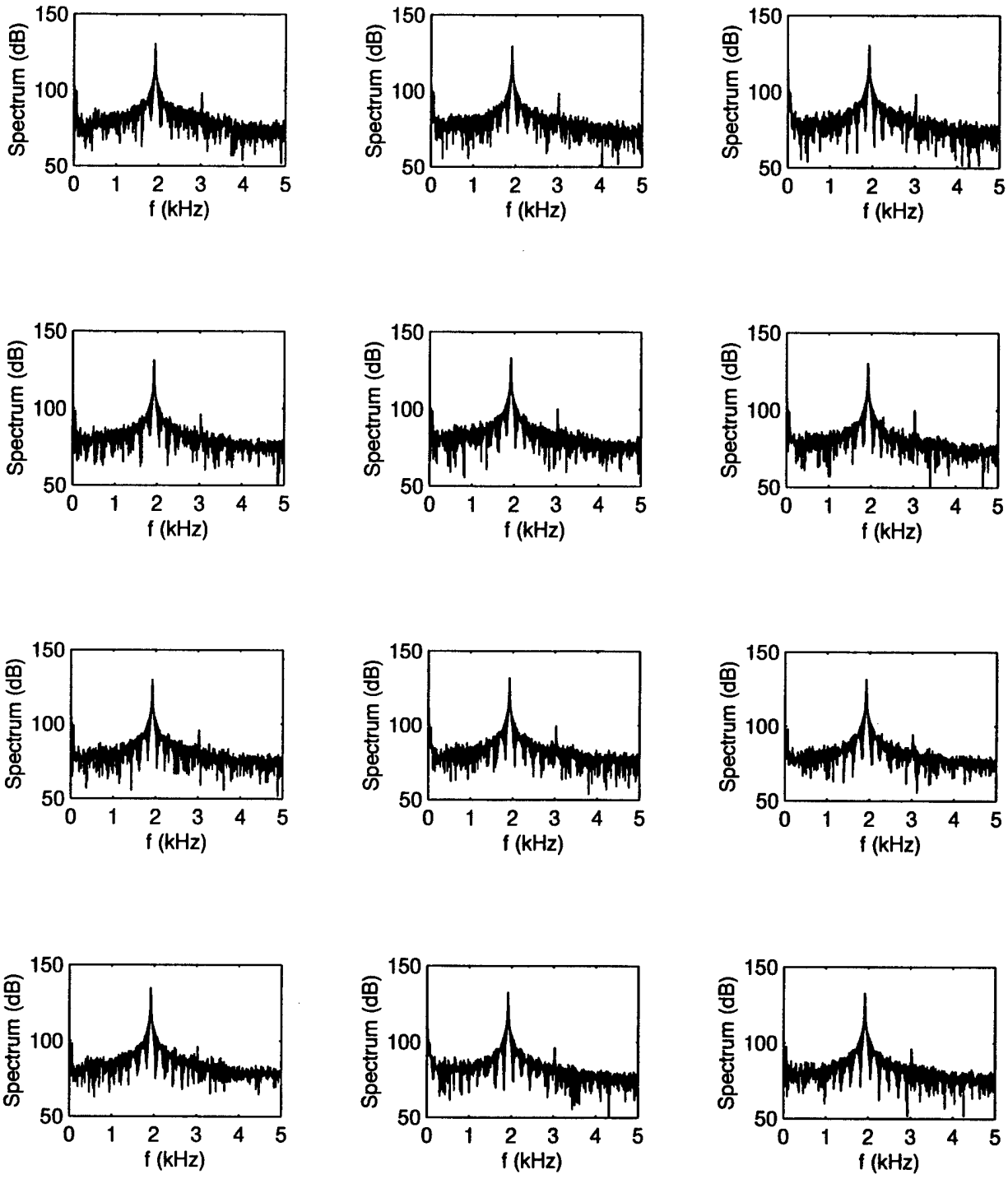

Figure 11. The spectra of the outputs of the twelve array elements in Block 1 of File 1.

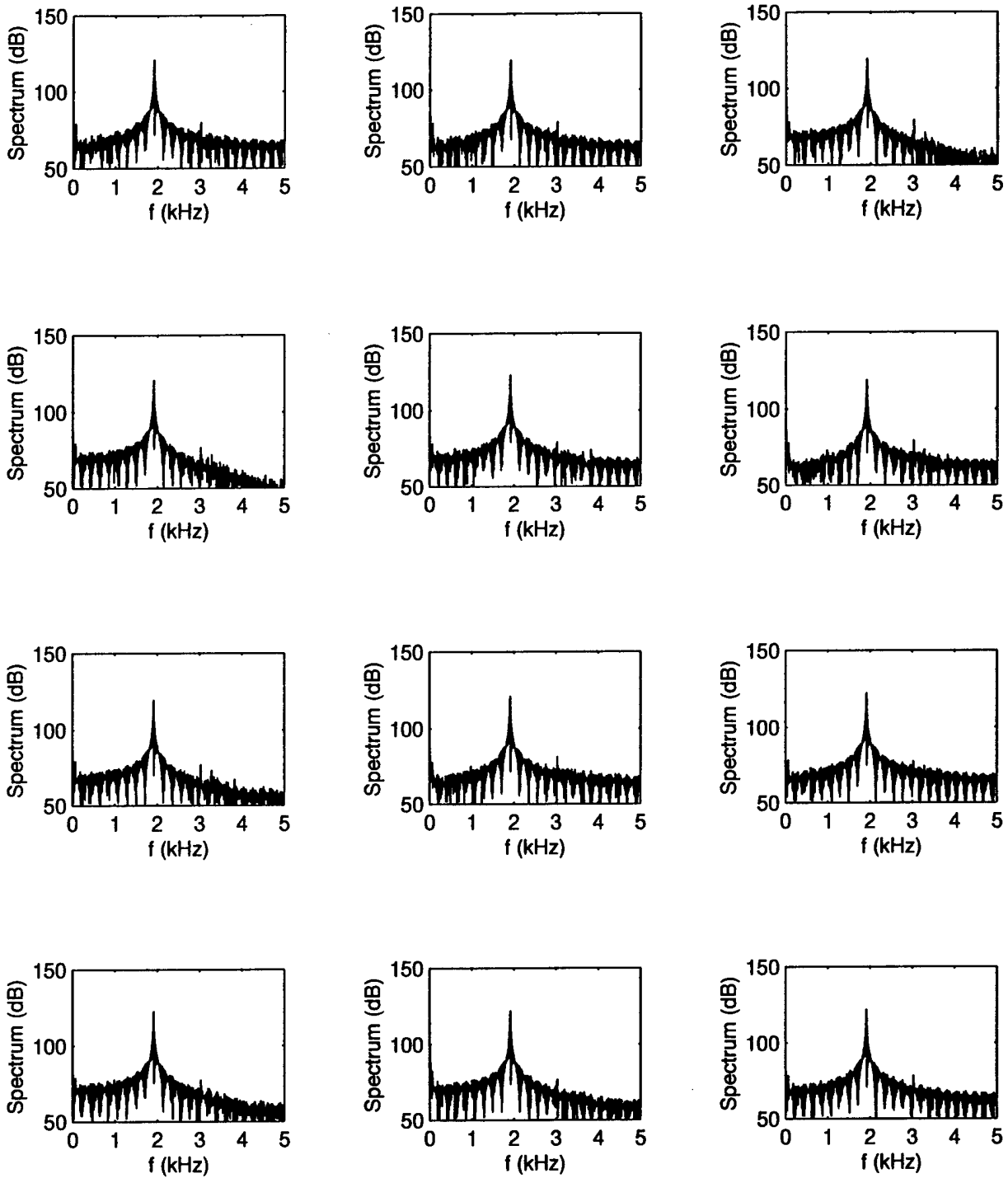

Figure 12. The spectra of the outputs of the twelve array elements in Block 1 of File 2.

Only 1000 array snapshots were used to calculate each Doppler spectrum, although each data block had 8000 snapshots. This number of snapshots was selected, because the bin width in the FFT spectrum must not be smaller than the frequency bandwidth of the received transmitter signal and the Doppler shift due to transmitter motion was changing with time.

To produce a spectrum, the sequence of 1000 real output amplitudes of an array element was augmented with 1048 zeros; the augmented sequence was converted to a 2048 point power spectrum, using the FFT; and the first 1024 amplitudes in the spectrum were plotted. The augmentation with zeros was necessary. Otherwise, picket fence effect and noise presence could combine to prevent the strongest amplitude from appearing at the same frequency bin in every spectrum. Only the first 1024 amplitudes were plotted, because the element output amplitudes were real and did not have quadrature components. Consequently, the spectrum was symmetrical about bin k=1, and the amplitudes for bins k and (2050-k) were the same.

Each FFT spectrum has 2048 frequency bins. These bins are identified with k=1 to 2048. The frequency at the k-th bin is 5.0781(k-1) Hz for k=1 to 1024 and 5.0781(k-2049) Hz for k=1025 to 2048. It is equal to $|f_s-f_o|$ where f_s is the signal frequency and f_o is the oscillator frequency.

4.2 Doppler Filtering

Doppler filtering was used to reduce each data block from 8000 array snapshots to eight new ones 30 dB stronger in SNR compared with the original snapshots. The procedure is given below.

Step 1.

Separate the data in each data block into eight sets with 1000 consecutive snapshots per set.

Step 2.

For each set,

(a) Augment the 1000 output amplitudes with 1048 zeros;

(b) Calculate the 2048 point complex FFT spectrum of the augmented

sequence; and

(c) Retain the first 1024 complex amplitudes.

Step 3.

Study the complex FFT spectrum calculated with the outputs of the first array element. Identify the signal bin as the bin with the largest power.

Step 4.

Construct a new array snapshot as

$$\mathbf{x}'' = (x_1'', x_2'', x_3'', \cdots, x_{12}'')^T \quad . \tag{4.1}$$

Denote the corresponding transmitter location by $\mathbf{r}''$.

In (4.1), x_1'' to x_{12}'' are the complex amplitudes in the signal bins in the FFT spectra calculated with the outputs of elements 1 to 12, respectively. The superscript 'T' denotes the transpose and the location $\mathbf{r}''$, where $\mathbf{r}''=(r'', \theta'', \psi'')$, denotes the average of the transmitter locations in the 1000 array snapshots.

4.3 File Size Reduction

This task is designed to reduce the size of each filtered file to M snapshots, with M=3600 for Files 1 to 5 and M=2435 for File 6. File 6 has a smaller M, because it has less than 3000 snapshots before reduction. In the following procedure, the set of array snapshots before reduction is denoted by $\{\mathbf{x}_1'', \mathbf{x}_2'', \mathbf{x}_3'', \cdots\}$ and the set after reduction is denoted by $\{\mathbf{x}_1', \mathbf{x}_2', \mathbf{x}_3', \cdots, \mathbf{x}_M'\}$.

Step 1.

Generate a set of M dummy bearings as

$$\tilde{\theta}_m = \theta_1 + 360(m-1)/M \quad . \qquad m=1,2,\cdots,M-1 \ , \tag{4.2}$$

where θ_1 is the bearing of the first snapshot in the filtered file.

Step 2.

In the set $\{\mathbf{x}''_1, \mathbf{x}''_2, \mathbf{x}''_3, \cdots\}$, identify the snapshot with bearing closest to $\tilde{\theta}_m$ as $\mathbf{x}'_m$. Denote the transmitter location of this snapshot by $\mathbf{r}'_m$.

The $\mathbf{r}'_m$ in Step 2 represents the set $(r'_m, \theta'_m, \psi'_m)$, where r'_m is the measured transmitter range.

4.4 Correction for Non-Planar Wavefront

Antenna arrays are normally calibrated to receive signals from remote sources. These sources produce planar signal wavefronts at the array. However, the wavefronts in $\{\mathbf{x}'_1, \mathbf{x}'_2, \mathbf{x}'_3, \cdots, \mathbf{x}'_M\}$ were not planar, because the transmitter range was 10 km or less. Given $\mathbf{x}'$ (snapshot $\mathbf{x}'_m$ with identification suppressed), we correct the deviation from a planar wavefront by replacing it with a new snapshot $\mathbf{x}$, where $\mathbf{x}=(x_1, x_2, \cdots, x_{12})^T$, constructed as

$$x_n = \{(s_n/r_t)\ \exp[j2\pi(s_n-r_t)/\lambda]\ x'_n\}\ a_n(\theta_t, \psi_t)\ , \qquad n=1,2,\cdots,12. \tag{4.3}$$

In this expression,

$\{s_1, s_2, s_3, \cdots, s_{12}\}$ = element distances from transmitter,

r_t = measured transmitter range from origin of coordinate system,

λ = signal wavelength
= 58.82 m,

and

$$a_n(\theta_t, \psi_t) = \exp[j2\pi(u_n\cos\psi_t\cos\theta_t - v_n\cos\psi_t\sin\theta_t + w_n\sin\psi_t)/\lambda]\ . \tag{4.4}$$

In (4.3), the factor (s_n/r_t) corrects the r^{-2} dependence of signal power on range, $\exp[j2\pi(s_n-r_t)/\lambda]$ equalizes the signal phases at the elements, and $a_n(\theta_t, \psi_t)$ is the n-th component of the array steering vector for direction (θ_t, ψ_t). In the absence of noise and interference, the

product inside the bracket { } is the same for all array elements and the source direction of **x** is determined by $a_n(\theta_t, \psi_t)$, n=1 to 12. The signal wavefront is planar in **x**.

5.0 CALIBRATION METHOD

A brief description of the calibration method in [1] is presented here. It includes the signal model used, the assumptions made, and the procedure for calculating the calibration matrix.

In the presentation, N denotes the number of array elements, the set $\{1, g_2, g_3, \cdots, g_N\}$ denotes the element gains, $\{0, \delta_2, \delta_3, \cdots, \delta_N\}$ denotes the element phases, $\{\mathbf{x}_1, \mathbf{x}_2, \mathbf{x}_3, \cdots, \mathbf{x}_M\}$ denotes M preprocessed array snapshots, and $\{(\theta_1, \psi_1), (\theta_2, \psi_2), (\theta_3, \psi_3), \cdots, (\theta_M, \psi_M)\}$ denotes the signal directions in the snapshots. The coefficients of a matrix **B**, for example, are denoted by $\{b_{pq}: p=1,2,\cdots; q=1,2,\cdots\}$. **B** is a normalized matrix if $b_{11}=1$.

The element gains and phases at array elements 2 to N are unknowns and are measured relative to those of the first element. They are independent of direction. Their deviations from unit gain and zero phase originate from mismatches in the cables and electronics at the elements.

5.1 Signal Model

In the signal model used, the set of M preprocessed array snapshots are associated with a set of M ideal array snapshots $\{\mathbf{y}_1, \mathbf{y}_2, \mathbf{y}_3, \cdots, \mathbf{y}_M\}$ given by

$$\mathbf{y}_m = \alpha_m \mathbf{v}_m, \qquad m=1,2,\cdots,M \ , \tag{5.1}$$

where α_m is the complex signal amplitude in snapshot $\mathbf{y}_m$, and $\mathbf{v}_m$ is the array steering vector for the corresponding source direction (θ_m, ψ_m). This expression assumes a perfectly calibrated array, a pure tone signal, no interaction among the array elements, no noise, and no interference.

The measured array snapshots are related to the ideal snapshots by

$$\mathbf{x}_m = \mathbf{\Gamma B}(\mathbf{y}_m + \mathbf{e}_m), \qquad m=1,2,\cdots,M \ , \tag{5.2}$$

where $\mathbf{\Gamma}$ is the matrix of element gains and phases and is given by

$$\mathbf{\Gamma} = \text{diag}\ \{1, g_2 \exp[j\delta_2], g_3 \exp[j\delta_3], \cdots, g_N \exp[j\delta_N]\} \ , \tag{5.3}$$

$\mathbf{B}$ is a normalized matrix related to the coupling among the array elements, and $\mathbf{e}_m$ is an error term representing the sum effect of noise, interfering signals, sensor misplacements, interactions between the array elements and local objects, etc..

The calibration matrix is defined as the normalized matrix $\mathbf{C}$ that, together with a set of amplitude estimates $\{\hat{\alpha}_1, \hat{\alpha}_2, \hat{\alpha}_3, \cdots, \hat{\alpha}_M\}$, minimizes the objective function

$$S = \sum_{m=1}^{M} |\mathbf{C}\mathbf{x}_m - \mathbf{y}_m|^2 \quad . \tag{5.4}$$

i.e.

$$\{\mathbf{C}, \hat{\boldsymbol{\alpha}}\} = \arg \min_{\mathbf{C}, \hat{\boldsymbol{\alpha}}} \{S\} \quad . \tag{5.5}$$

Function S depends on the unknowns $\hat{\alpha}_1$ to $\hat{\alpha}_M$ through (5.1). The '$\hat{}$' denotes the estimate. For convenience, $\hat{\boldsymbol{\alpha}}$ has been used to denote the set $\{\hat{\alpha}_1, \hat{\alpha}_2, \hat{\alpha}_3, \cdots, \hat{\alpha}_M\}$.

Because $\mathbf{C}$ is normalized, it satisfies the condition

$$c_{11} = 1.0 \quad . \tag{5.6}$$

This condition ensures that $\mathbf{C}$ is unique. It also excludes the trivial solution $\{\mathbf{C}=\mathbf{0}_N, \hat{\alpha}_1=\hat{\alpha}_2=\cdots=\hat{\alpha}_M=0\}$, where $\mathbf{0}_N$ denotes the N×N null matrix.

5.2 Assumptions

The following assumptions are made in the development of the calibration method:

1. The array elements are narrowband;

2. The mutual coupling among the elements can be approximated by a matrix operation;

3. The signal source (the transmitter) moves over a wide range of directions during the calibration experiment;

4. The number of array snapshots in the calibration data is reasonably large;

5. A preliminary calibration has been carried out to equalize the element gains and phases of the antenna array. After this calibration, the global maximum of every antenna beam pattern is the maximum closest to the beam steering direction; and

6. The signal-to-interference-plus-noise ratio (SINR) in the array snapshots is high enough for estimating the complex signal amplitudes in the snapshots.

5.3 Computation of Calibration Matrix

The calibration matrix $\mathbf{C}$ is obtained by iteration, assuming that only one signal source is present in every array snapshot. In each iteration, the sum S is initially minimized with respect to the estimates of signal amplitudes. Then it is minimized with respect to $\mathbf{C}$. The procedure is based on the following observations:

A. If $\mathbf{C}_{k-1}$ is an estimate of $\mathbf{C}$ and

$$\mathbf{z}_m = \mathbf{C}_{k-1}\mathbf{x}_m \ , \tag{5.7}$$

the least square estimate of α_m is given by

$$\hat{\alpha}_m = \mathbf{v}_m^H \mathbf{z}_m / |\mathbf{v}_m|^2 \ , \tag{5.8}$$

and the corresponding estimate of $\mathbf{y}_m$ is given by

$$\hat{\mathbf{y}}_m = \hat{\alpha}_m \mathbf{v}_m \ . \tag{5.9}$$

B. Given $\{\hat{\mathbf{y}}_1, \hat{\mathbf{y}}_2, \cdots, \hat{\mathbf{y}}_M\}$, one can get a new normalized least square estimate of $\mathbf{C}$ by solving the equation

$$\mathbf{C}_k \mathbf{X} = \hat{\mathbf{Y}} \tag{5.10}$$

as

$$\mathbf{C}_k = (\hat{\mathbf{Y}}\hat{\mathbf{Y}}^H)(\mathbf{X}\hat{\mathbf{Y}}^H)^{-1} \ , \tag{5.11}$$

and then impose the condition (5.6) on $\mathbf{C}_k$.

In these expressions, $\mathbf{X}$ denotes the N×M matrix $(\mathbf{x}_1, \mathbf{x}_2, \cdots, \mathbf{x}_M)$, $\hat{\mathbf{Y}}$ denotes $(\hat{\mathbf{y}}_1, \hat{\mathbf{y}}_2, \cdots, \hat{\mathbf{y}}_M)$, and the superscript 'H' denotes the conjugate-transpose. The inverse $(\mathbf{X}\hat{\mathbf{Y}}^H)^{-1}$ exists, because of Assumption 3.

C. The initialization $\mathbf{C}_0=\mathbf{I}_N$, where $\mathbf{I}_N$ is an N×N identify matrix, is equivalent to using the original data in the first iteration, where k=1.

D. Let a difference matrix be defined as

$$\mathbf{D}_k = \mathbf{C}_k - \mathbf{C}_{k-1}. \tag{5.12}$$

Let the magnitude of the largest coefficient in this matrix be given by ϵ_k, i.e.,

$$\epsilon_k = \max\{|d_{pq}| : p,q=1,2,\cdots,N\} , \tag{5.13}$$

Where each d_{pq} is a coefficient of $\mathbf{D}_k$. One can terminate the iteration if (a) $\epsilon_k<\epsilon'$, where ϵ' is a prespecified small value or (b) $\epsilon_k>\epsilon_{k-1}$. In case (a), the iteration has converged to a prespecified level. In (b), the convergence condition is not satisfied yet, but more iterations do not guarantee more accurate estimates of $\mathbf{C}$.

In a preliminary study with File 2 and 100 iterations, ϵ_k decreased steadily from 0.44064 for k=1 to 0.00035 for k=23. It then varied randomly between 0.00016 to 0.00063 for the next 77 iterations. With File 6, ϵ_k decreased steadily from 2.70607 for k=1 to 0.06215 for k=14. It then varied randomly between 0.02910 and 0.15553 in the next 86 iterations.

The computation of the calibration matrix is described below. There are six steps.

Step 1.

Let k=1 and $\mathbf{C}_0=\mathbf{I}_N$.

Step 2.

Calculate $\{\hat{\mathbf{y}}_1, \hat{\mathbf{y}}_2, \cdots, \hat{\mathbf{y}}_M\}$ with (5.7) to (5.9).

Step 3.

Calculate $\mathbf{C}_k$ with (5.11)

Step 4.

Impose condition (5.6) on $\mathbf{C}_k$.

Step 5.

Calculate ϵ_k with (5.12) and (5.13).

Step 6.

If $\epsilon_k<0.0005$ or $\epsilon_k>\epsilon_{k-1}$,
terminate the iterations and identify $\mathbf{C}_k$ as $\mathbf{C}$.

Else,
replace k by k+1 and return to Step 2.

A few notes are in order. Firstly, in Step 2 of the last iteration, $\hat{\alpha}_1$ to $\hat{\alpha}_M$ are estimates of the complex signal amplitudes in $\mathbf{x}_1$ to $\mathbf{x}_M$, respectively. Secondly, given a calibration matrix $\mathbf{C}$ and a measured array snapshot $\mathbf{x}$, the corresponding calibrated array snapshot, denoted by $\mathbf{x}^c$, is given by

$$\mathbf{x}^c = \mathbf{C}\mathbf{x} \ . \tag{5.14}$$

Thirdly, from (5.2) and (5.4), the normalized inverse of $\mathbf{C}$, denoted by $\tilde{\mathbf{C}}^{-1}$, is related to the product $\mathbf{\Gamma B}$ by

$$\tilde{\mathbf{C}}^{-1} = b_{11}^{-1}(\hat{\mathbf{\Gamma B}}) \ , \tag{5.15}$$

where b_{11} is the first diagonal element of $\mathbf{B}$. Finally, if

$$b_{11} = b_{22} = \cdots = b_{NN} \quad \text{(Assumption)} \ , \tag{5.16}$$

one can estimate $\boldsymbol{\Gamma}$ and the product $b_{11}^{-1}\mathbf{B}$ as

$$\hat{\boldsymbol{\Gamma}} = \text{matrix } \tilde{\mathbf{C}}^{-1} \text{ with off-diagonal elements equated to zero} \ , \tag{5.17}$$

$$\widehat{b_{11}^{-1}\mathbf{B}} = \hat{\boldsymbol{\Gamma}}^{-1}\tilde{\mathbf{C}}^{-1} \ . \tag{5.18}$$

6.0 CALIBRATION MATRICES

Each one of the six preprocessed data files has been used to calculate a calibration matrix $\mathbf{C}$, a normalized inverse $\tilde{\mathbf{C}}^{-1}$ of $\mathbf{C}$, an estimate of $\boldsymbol{\Gamma}$, and an estimate of the product $b_{11}\mathbf{B}$. Due to the hugh quantity of data generated, only the notable observations are presented here. In the discussions, $\mathbf{C}(2)$, for example, denotes the matrix calculated with File 2. The corresponding estimate of $b_{11}^{-1}\mathbf{B}$ is denoted by $\hat{b}_{11}^{-1}\mathbf{B}(2)$.

The assumption (5.16) is only approximately valid here. However, the results obtained with (5.17) and (5.18) are included in the discussions, because the estimates $\hat{\boldsymbol{\Gamma}}$ and $\hat{b}_{11}^{-1}\mathbf{B}$ contain special features that can be identified with the antenna array configuration and its environment.

The preprocessed data files are used in the calculation, because they have many desirable properties. Firstly, in a preliminary study, the SINRs in the individual array snapshots are usually over 15 dB. Secondly, the number of snapshots per file is not too large and not too small. Thirdly, the signal source (the transmitter) circles the array once in the file. Fourthly, the snapshots are approximately equally spaced in source bearings.

The estimates of element gains and phases are in Tables 3 and 4, respectively. They were calculated with (5.3) and matrices $\hat{\boldsymbol{\Gamma}}(1)$ to $\hat{\boldsymbol{\Gamma}}(6)$. In Tables 5 to 6 are the magnitudes and phases of the coefficients in $\mathbf{C}(2)$. Tables 7, 8, 9 and 10 contain the magnitudes of the coefficients in $\hat{b}_{11}^{-1}\mathbf{B}(2)$, the difference $\mathbf{C}(2)-\mathbf{C}(3)$, $\mathbf{C}(4)$, and $\mathbf{C}(6)$, respectively. Some notable observations are given below.

1. In Table 3, many gain estimates are less than 0.8 or larger than 1.2. In Table 4, many phase estimates are less than -10° or more than 10°. In Table 5, four coefficients in the main diagonal are less than 0.8. In Table 6, three phase estimates in the main diagonal deviate from zero by more than 10°.

   Remark: It appears that there were difficulties in the initial calibration of the antenna array.

2. In Table 3, the gain estimates from Files 2 and 3 are essentially the same and differ by 0.034 or less. In Table 4, with the exception of element #7, the phase estimates from these files differ by 1° or less.

   Remark: Files 2 and 3 were collected with the same source elevations and ranges. The above difference in the estimates of gains and phases indicates that measurement errors, including noise and interference effects, were relatively small.

3. In Tables 3 and 4, the gain and phase estimates calculated with File 6 differ noticeably from those calculated with Files 2 and 3.

   Remark: The result is not unexpected. It was noted in Chapter 4 that there are large measurement errors in File 6 and that these errors cannot be suppressed by data preprocessing.

4. In Table 7, the magnitudes of many off-diagonal coefficients are larger than 0.1.

   Remark: This property indicates strong coupling among the array elements or between the elements and local objects, or both.

5. In Table 7, the magnitudes for $(p,q)=(1,2)$ and $(2,1)$ are 0.238 or larger. Those for $(p,q)=(7,8)$ and $(8,7)$ are significantly smaller and are 0.041 or less.

   Remark: The results for $(p,q)=(1,2)$ and $(2,1)$ are expected. From Table 1, elements #1 and #2 are separated by 6.53m, which is approximately 0.11 wavelength at 5.1 MHz. With this separation, one expects very strong coupling between the two elements. Those for $(p,q)=(7,8)$ and $(8,7)$ are unexpected, because elements #7 and #8 are separated by 6.53m also. The significantly smaller values indicate very strong interactions between the elements and local objects.

6. In Table 7, many off-diagonal coefficients in the lower left corner are larger than 0.1 while the diagonally opposite ones in the upper right corner are less than 0.02. The coefficients with $p \geq 9$ and $q \leq 4$ (in the lower left corner) are noticeable larger than those with $p \leq 4$ and $q \geq 9$ (upper right corner).

Remark: The true reason is unknown. These properties may have something to do with the absence of ground radial wires in elements #9 to #12. Computer simulations show that one can generate a matrix $b_{11}\hat{}^{-1}\mathbf{B}$ with this property by introducing strong interactions between these elements and local objects.

7. In Table 8, the magnitude of first coefficient in the main diagonal of the difference $\mathbf{C}(2)-\mathbf{C}(3)$ is zero. The magnitudes of the other coefficients are between 0.012 and 0.025.

   Remarks: The first coefficient is zero, because $\mathbf{C}(2)$ and $\mathbf{C}(3)$ both satisfy condition (5.6). The other coefficients indicate that the errors in the main diagonal of Table 5 are small and are unlikely to exceed 0.03.

8. In Table 8, five coefficients in the lower left corner, where $p \geq 9$ and $q \leq 4$, are larger than 0.020.

   Remark: These values are rather large compared with the other off-diagonal coefficients. They may be related to the absence of ground radial wires for elements #9 to #12.

9. The values in the upper right corner of Table 10 are noticeably larger than those in Table 9.

   Remark: The results are expected. The reasons are the same as those in Observation #3.

Element	Element Gain Estimate					
	File=1 (ψ=4.5°)	2 (11°)	3 (11°)	4 (18°)	5 (31°)	6 (49°)
1	1.000	1.000	1.000	1.000	1.000	1.000
2	1.352	1.430	1.408	1.293	1.433	0.918
3	0.870	0.922	0.888	1.093	1.672	1.218
4	1.187	1.261	1.249	1.240	1.691	1.958
5	1.218	1.235	1.225	1.133	1.621	0.810
6	1.105	1.200	1.180	1.116	1.177	0.663
7	1.088	1.139	1.128	0.978	1.407	0.410
8	1.127	1.231	1.210	1.222	1.519	1.143
9	0.988	1.200	1.183	1.215	1.611	0.895
10	1.079	1.093	1.071	1.064	1.311	0.719
11	1.075	1.116	1.099	1.134	1.498	0.861
12	1.012	1.030	1.013	0.998	1.258	0.773

Table 3: Estimates of element gains.

Element	Element Phase Estimate (deg)					
	File=1 (ψ=4.5°)	2 (11°)	3 (11°)	4 (18°)	5 (31°)	6 (49°)
1	0	0	0	0	0	0
2	24	22	23	33	17	-12
3	32	6	6	25	14	121
4	12	10	11	7	15	-13
5	11	10	11	20	6	-8
6	11	12	13	17	14	-4
7	14	7	15	22	13	-2
8	10	12	12	18	13	-1
9	8	10	11	16	8	-7
10	0	-1	0	7	0	-11
11	-21	-22	-21	-15	-23	-34
12	-4	-5	-5	1	-4	10

Table 4. Estimates of element phases in degrees.

p	q=1	q=2	3	4	5	6	7	8	9	10	11	12
1	1.000	0.279	0.375	0.270	0.090	0.051	0.029	0.030	0.002	0.015	0.009	0.003
2	0.237	0.671	0.371	0.245	0.085	0.047	0.011	0.022	0.005	0.012	0.005	0.012
3	0.151	0.183	1.031	0.125	0.062	0.038	0.004	0.007	0.005	0.009	0.005	0.016
4	0.106	0.120	0.130	0.766	0.058	0.040	0.010	0.016	0.005	0.009	0.005	0.014
5	0.071	0.146	0.168	0.123	0.791	0.026	0.007	0.045	0.014	0.017	0.009	0.007
6	0.075	0.099	0.094	0.050	0.015	0.818	0.018	0.017	0.006	0.017	0.010	0.010
7	0.140	0.175	0.181	0.090	0.049	0.037	0.858	0.035	0.013	0.014	0.014	0.008
8	0.059	0.064	0.071	0.031	0.051	0.015	0.020	0.795	0.007	0.011	0.008	0.005
9	0.066	0.074	0.089	0.069	0.017	0.051	0.087	0.025	0.817	0.022	0.018	0.003
10	0.133	0.208	0.332	0.273	0.127	0.045	0.072	0.034	0.025	0.897	0.028	0.022
11	0.053	0.112	0.104	0.091	0.008	0.038	0.033	0.033	0.039	0.022	0.878	0.014
12	0.124	0.158	0.179	0.171	0.115	0.095	0.094	0.071	0.028	0.035	0.032	0.950

Table 5. Magnitudes of coefficients in matrix **C**(2) calculated with File 2.

p	q=1	q=2	3	4	5	6	7	8	9	10	11	12
1	0	-149	27	-160	17	-167	-146	47	-55	-104	-26	-135
2	44	-28	25	-166	14	-180	-180	42	-103	-81	-14	-66
3	37	-157	-4	173	14	179	38	48	-126	-1	60	-34
4	51	-148	24	-9	24	-176	43	-160	158	14	40	-25
5	-15	159	-30	144	-8	-173	25	-149	180	31	47	-28
6	-91	121	-66	134	115	-10	163	-120	-115	55	40	-7
7	-161	21	-160	25	-146	158	-12	112	-130	120	-168	-153
8	-151	32	-169	-12	-157	160	-19	-9	-92	126	-152	171
9	-108	98	-83	141	-153	-148	-165	1	-8	158	-165	34
10	-87	105	-47	141	-12	163	41	-113	-150	3	52	-87
11	-100	76	-110	63	-39	75	109	-32	-171	11	24	-107
12	47	-124	101	-47	147	-38	-143	57	-24	-175	-155	8

Table 6. Phases of coefficients in matrix **C**(2).

p	q=1	q=2	3	4	5	6	7	8	9	10	11	12
1	1.000	0.238	0.522	0.277	0.105	0.061	0.035	0.033	0.003	0.018	0.011	0.004
2	0.293	1.000	0.508	0.247	0.098	0.056	0.017	0.024	0.005	0.014	0.006	0.014
3	0.192	0.159	1.000	0.128	0.072	0.044	0.007	0.007	0.004	0.010	0.004	0.020
4	0.132	0.102	0.175	1.000	0.066	0.048	0.012	0.019	0.006	0.010	0.005	0.016
5	0.105	0.150	0.273	0.147	1.000	0.036	0.009	0.060	0.017	0.020	0.010	0.009
6	0.085	0.084	0.126	0.054	0.019	1.000	0.018	0.021	0.006	0.020	0.013	0.012
7	0.171	0.144	0.231	0.079	0.054	0.045	1.000	0.041	0.017	0.016	0.015	0.009
8	0.066	0.044	0.075	0.018	0.059	0.019	0.026	1.000	0.010	0.014	0.009	0.006
9	0.092	0.074	0.145	0.092	0.014	0.072	0.105	0.025	1.000	0.027	0.022	0.004
10	0.143	0.153	0.410	0.253	0.142	0.044	0.079	0.033	0.023	1.000	0.031	0.023
11	0.069	0.105	0.164	0.106	0.012	0.046	0.035	0.036	0.044	0.024	1.000	0.016
12	0.132	0.109	0.178	0.141	0.117	0.095	0.095	0.071	0.026	0.036	0.034	1.000

Table 7. Magnitudes of coefficients in the estimate $\hat{b}_{11}^{-1}\mathbf{B}(2)$ calculated with File 2.

p	q=1	q=2	3	4	5	6	7	8	9	10	11	12
1	0.000	0.017	0.013	0.007	0.004	0.004	0.001	0.002	0.000	0.002	0.001	0.002
2	0.005	0.015	0.005	0.005	0.002	0.003	0.001	0.002	0.001	0.002	0.001	0.002
3	0.010	0.014	0.025	0.011	0.001	0.003	0.004	0.001	0.000	0.001	0.001	0.002
4	0.009	0.010	0.012	0.016	0.002	0.004	0.005	0.001	0.000	0.001	0.001	0.002
5	0.006	0.006	0.011	0.011	0.012	0.003	0.005	0.004	0.001	0.001	0.001	0.001
6	0.009	0.008	0.008	0.007	0.003	0.015	0.004	0.005	0.001	0.002	0.001	0.001
7	0.006	0.007	0.009	0.008	0.002	0.001	0.014	0.007	0.001	0.001	0.001	0.001
8	0.004	0.005	0.007	0.005	0.002	0.001	0.006	0.011	0.001	0.001	0.001	0.001
9	0.010	0.017	0.027	0.022	0.003	0.002	0.005	0.004	0.014	0.003	0.000	0.003
10	0.016	0.027	0.033	0.026	0.006	0.006	0.004	0.003	0.003	0.020	0.004	0.002
11	0.008	0.012	0.027	0.021	0.006	0.004	0.006	0.005	0.002	0.003	0.020	0.004
12	0.001	0.006	0.008	0.007	0.003	0.009	0.007	0.004	0.000	0.003	0.001	0.019

Table 8. Magnitudes of coefficients in the difference **C**(2)-**C**(3).

p	q=1	q=2	3	4	5	6	7	8	9	10	11	12
1	1.000	0.412	0.511	0.364	0.109	0.065	0.038	0.023	0.005	0.007	0.006	0.021
2	0.243	0.757	0.349	0.218	0.091	0.050	0.026	0.021	0.007	0.011	0.006	0.022
3	0.055	0.017	0.879	0.136	0.077	0.062	0.042	0.045	0.008	0.020	0.010	0.008
4	0.027	0.061	0.138	0.749	0.086	0.069	0.039	0.042	0.008	0.017	0.010	0.002
5	0.153	0.314	0.432	0.333	0.811	0.039	0.009	0.030	0.005	0.018	0.009	0.005
6	0.159	0.247	0.292	0.195	0.040	0.833	0.028	0.030	0.007	0.020	0.007	0.013
7	0.106	0.112	0.113	0.082	0.040	0.039	0.943	0.043	0.005	0.010	0.012	0.015
8	0.092	0.103	0.003	0.054	0.033	0.030	0.059	0.755	0.002	0.011	0.011	0.013
9	0.122	0.197	0.215	0.176	0.039	0.061	0.039	0.066	0.763	0.039	0.018	0.014
10	0.161	0.267	0.354	0.259	0.091	0.054	0.061	0.030	0.029	0.871	0.019	0.023
11	0.035	0.113	0.142	0.180	0.026	0.076	0.021	0.040	0.031	0.040	0.817	0.016
12	0.069	0.180	0.209	0.195	0.091	0.063	0.156	0.118	0.035	0.022	0.017	0.929

Table 9. Magnitudes of coefficients in C(4).

p	q=1	q=2	3	4	5	6	7	8	9	10	11	12
1	1.000	0.248	0.841	0.700	0.145	0.042	0.216	0.292	0.037	0.012	0.041	0.021
2	0.231	0.655	0.940	0.746	0.215	0.096	0.141	0.203	0.025	0.020	0.037	0.016
3	1.117	1.964	2.753	1.493	0.297	0.073	0.082	0.102	0.014	0.047	0.020	0.019
4	0.983	1.621	1.711	0.902	0.296	0.103	0.183	0.168	0.018	0.043	0.014	0.021
5	0.558	1.050	1.505	1.057	0.962	0.131	0.267	0.277	0.041	0.029	0.019	0.019
6	0.783	1.393	1.644	1.256	0.376	1.297	0.248	0.260	0.050	0.037	0.015	0.007
7	1.094	1.641	1.179	0.599	0.173	0.151	1.580	0.428	0.018	0.037	0.006	0.021
8	1.123	1.786	1.654	1.006	0.064	0.016	0.490	0.583	0.025	0.034	0.002	0.016
9	1.067	1.583	1.369	0.919	0.219	0.155	0.412	0.345	0.896	0.027	0.020	0.005
10	0.953	1.651	2.157	1.648	0.590	0.311	0.601	0.440	0.042	1.120	0.020	0.051
11	0.909	1.070	0.504	0.367	0.125	0.016	0.259	0.146	0.089	0.075	0.936	0.042
12	2.228	3.984	4.722	3.361	0.682	0.320	0.617	0.587	0.035	0.202	0.045	1.061

Table 10. Magnitudes of coefficients in **C**(6).

7.0 EVALUATION OF CALIBRATION METHOD

Matrix **C**(2), the calibration matrix calculated with File 2, was used to calibrate the array snapshots in the other files. The effect of calibration on the performance of the antenna array was then studied. This study included the antenna array beam patterns, the accuracy of direction estimates, and the resolution of signal directions.

It is preferable to use **C**(2) or **C**(3) to calibrate the array snapshots and we have arbitrarily chosen **C**(2). Matrices **C**(2) and **C**(3) are essentially the same and are generated with Files 2 and 3, respectively. In Table 2, these files have the same nominal transmitter elevations and ranges (radii). Therefore, we get the best performance improvements the calibration method can provide when **C**(2) is used to calibrate File 3 or **C**(3) is used to calibrate File 2.

File 6 was included in the evaluation. However, we avoid making comments on the positive results, if any, obtained. As noted at the beginning of Chapter 4, these results are unreliable, because of large measurement errors associated with the short transmitter range and the high elevation angles.

7.1 Effect on Antenna Beam Patterns

The one-way ideal measured and calibrated beam patterns of the antenna array are studied here. A one-way pattern shows the dependence of the array output power on signal source direction (θ_s, ψ_s), given that the source is in the farfield zone of the array, and the signal power at the array elements is kept independent of the direction (θ_s, ψ_s). This pattern depends on the beam steering direction, denoted by (θ_B, ψ_B), and is usually normalized to unit power at the global maximum. An ideal beam pattern is a pattern produced with the ideal array snapshots given by (5.1).

For the sake of convenience in comparing beam patterns, this study chose beam elevation angles that were equal to the nominal source elevations in the data files used to produce the patterns. With these choices, there is some assurance that the main peaks of the ideal, measured and calibrated beam patterns would be close to the beam steering

directions.

The calculation of beam patterns must take into consideration that the signal power in the array snapshots is not fixed in every data file. There are two reasons. Firstly, as one can observe from Figs. 3 to 8, the aircraft flight paths were not perfect circles about the vertical W-axis of the UVW-coordinate system. Deviations from the circular path produced variations of signal power at the array elements. Secondly, because of air turbulence behind an aircraft, the transmitter orientation was not fixed relative to the aircraft. Changes in transmitter orientations also produced variations in signal powers at the array elements.

Here, we attempt to suppress the dependence of signal power on source direction by normalizing separately the measured and calibrated array snapshots, which are complex vectors with N components, to vectors with unit magnitudes before using them in the calculations.

The three-steps procedure described below was used to calculate the beam patterns. In Step 2, M is the number of array snapshots in a preprocessed file, the set $\{(\theta_1,\psi_1),(\theta_2,\psi_2),\cdots,(\theta_M,\psi_M)\}$ denotes the source directions, $\{\mathbf{x}_1,\mathbf{x}_2,\cdots,\mathbf{x}_M\}$ denotes the preprocessed snapshots, and $\{\mathbf{x}_1^c,\mathbf{x}_2^c,\cdots,\mathbf{x}_M^c\}$ denotes the corresponding calibrated snapshots. These calibrated snapshots were calculated with (5.14) and the matrix $\mathbf{C}(2)$.

Step 1.

Specify the beam steering direction $\{\theta_B,\psi_B\}$.

Denote the corresponding array steering vector by $\mathbf{a}(\theta_B,\psi_B)$.

Step 2.

For m=1,2,$\cdots$,M,

(a) Calculate two unit-magnitude vectors $\tilde{\mathbf{x}}_m$ and $\tilde{\mathbf{x}}_m^c$ as

$$\tilde{\mathbf{x}}_m = \mathbf{x}_m / |\mathbf{x}_m| \ , \tag{7.1}$$

$$\tilde{\mathbf{x}}_m^c = \mathbf{x}_m^c / |\mathbf{x}_m^c| \ , \tag{7.2}$$

(b) Calculate the beam amplitudes in the ideal, measured and

calibrated beam patterns as

$$B_{ideal}(\theta_B,\psi_B;\theta_m,\psi_m) = \left|\mathbf{a}^H(\theta_B,\psi_B)\,\mathbf{a}(\theta_m,\psi_m)\right|^2 , \tag{7.3}$$

$$B_{meas}(\theta_B,\psi_B;\theta_m,\psi_m) = \left|\mathbf{a}^H(\theta_B,\psi_B)\,\tilde{\mathbf{x}}_m\right|^2 , \tag{7.4}$$

$$B_{cal}(\theta_B,\psi_B;\theta_m,\psi_m) = \left|\mathbf{a}^H(\theta_B,\psi_B)\,\tilde{\mathbf{x}}_m^c\right|^2 , \tag{7.5}$$

Step 3

(a) Find the largest amplitude in the set $\{B_{ideal}(\theta_B,\psi_B;\theta_m,\psi_m): m=1,2,\cdots,M\}$, which is calculated with (7.3). Use it to divide every amplitude in this set.

(b) Repeat with the other two sets calculated with (7.4) and (7.5).

Figs. 13 and 14 to 17 contain some results that are typical of the beam patterns obtained with Files 1 and 3 to 6, respectively. They are obtained with the beam elevation ψ_B equated to the nominal source elevations in Table 2 and the beam bearing arbitrarily assigned as $\theta_B=45°$. Each figure is divided into two halves: the upper half shows the patterns for all source bearings, and the lower half is a magnification of the section with $0°\le\theta_s<90°$. Vertical lines have been drawn through the source bearing $\theta_s=\theta_B$ to facilitate the study of the patterns in this region. The figures show the dependence of beam amplitudes on source bearing θ_s for $\theta_B=45°$ and $\psi_B=\psi_s=4.5°,11°,18°,31°,49°$. Some notable observations are given below:

1. The main peaks of the ideal beam patterns, drawn in solid lines, in the upper halves of Figs. 13 to 17 are centred at $\theta_s=45°$, the bearing of the beam steering direction. Up to eleven sidelobes are present. Some gradually merge together as the beam elevation increases. The peak values of many sidelobes are rather high and are larger than -10 dB.

   Remark: The above properties of the ideal beam patterns are determined by the design of the antenna array. They have nothing to

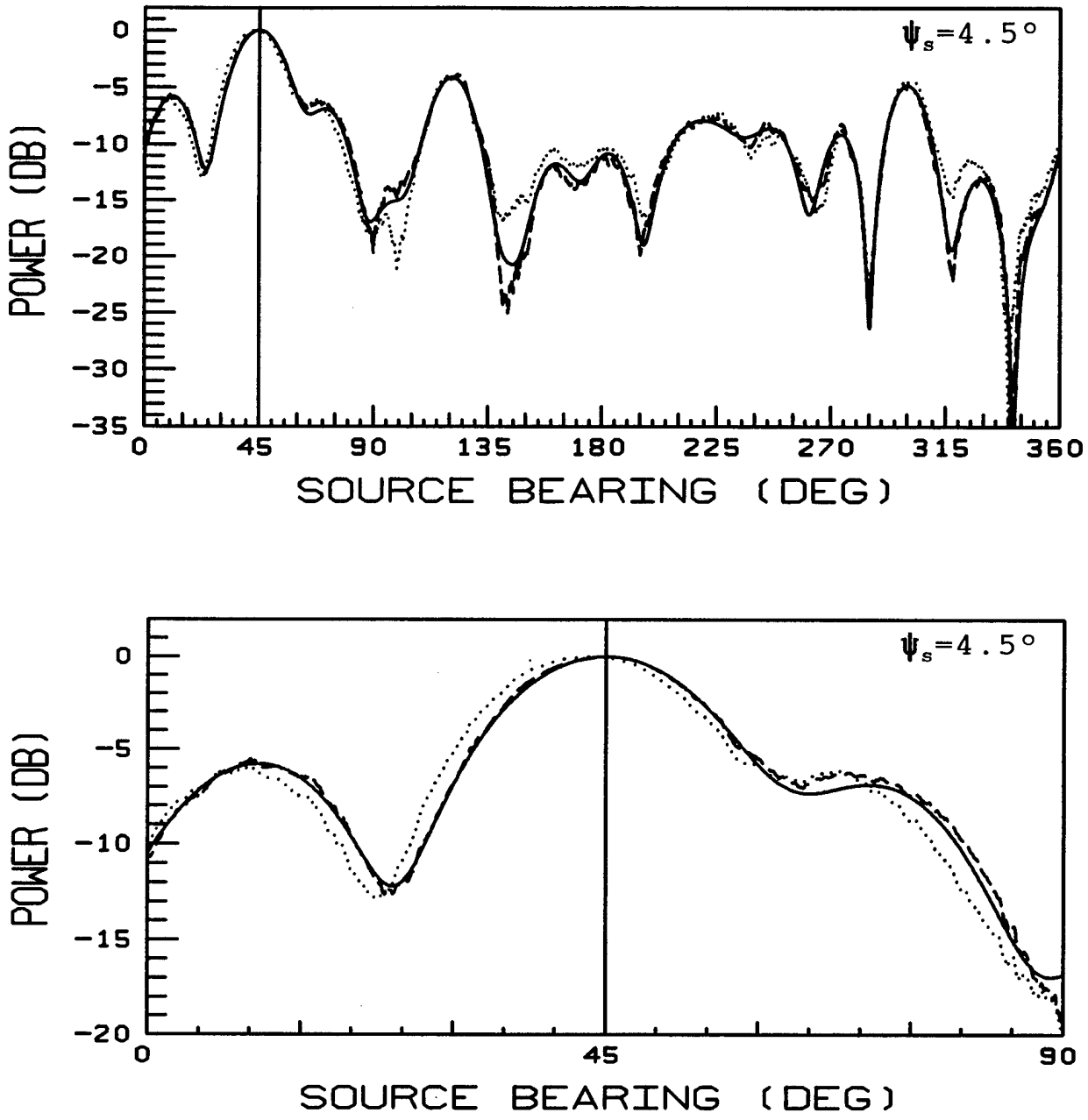

Fig. 13 The ideal (solid line), measured (dotted) and calibrated (broken) array beam patterns for beam steering direction (θ,ψ)= (45°,4.5°) and signal source elevation ψ_s=4.5. The lower figure is a magnification of the section with source bearing 0° to 90° and the vertical lines are drawn through the beam bearing θ=45°. File 1 has been used to produce the figure.

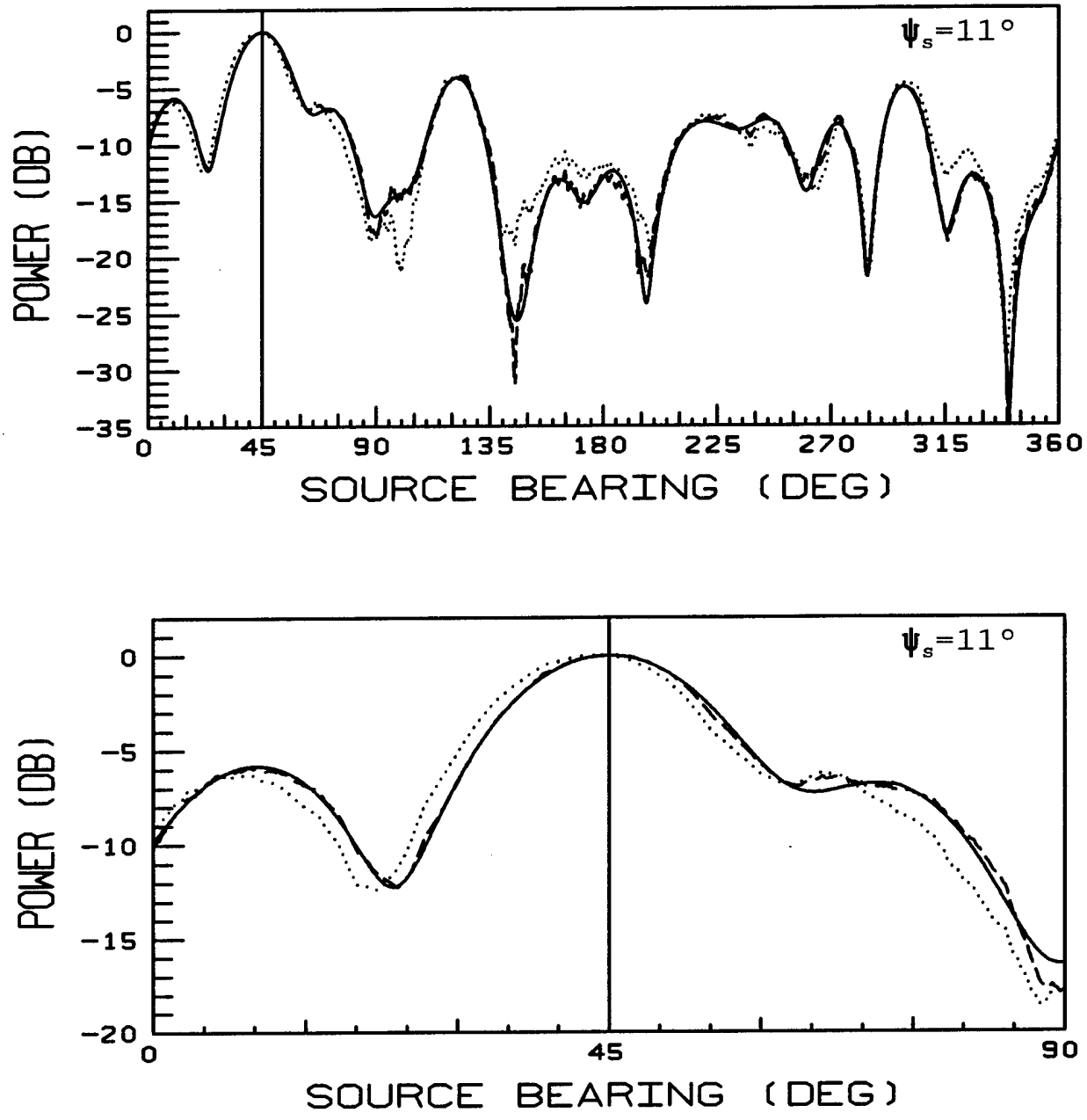

Fig. 14 The ideal (solid line), measured (dotted) and calibrated (broken) array beam patterns for beam steering direction (θ,ψ)= (45°,11°). File 3, where ψ_s=11°, has been used.

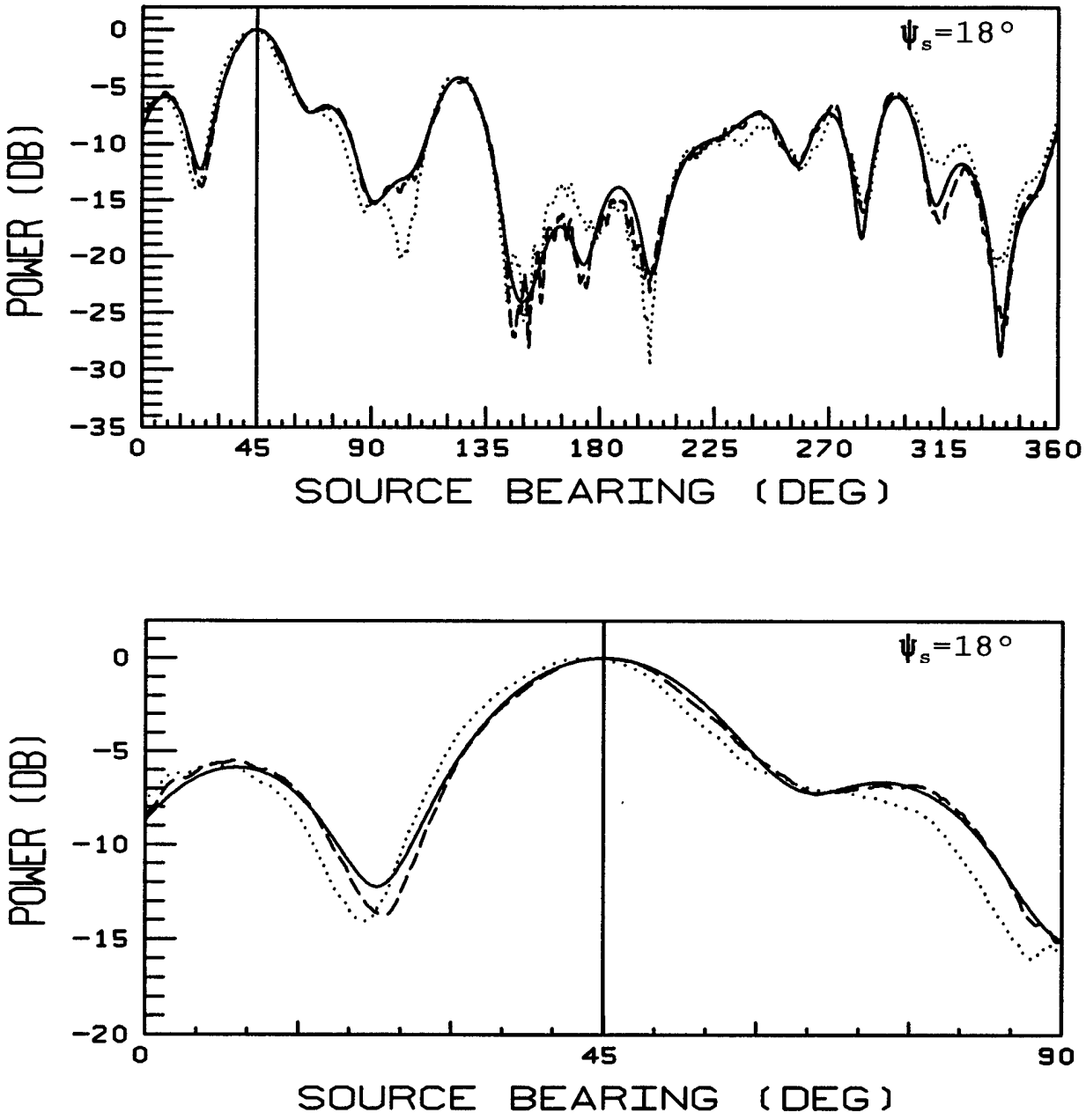

Fig. 15 The ideal (solid line), measured (dotted) and calibrated (broken) array beam patterns for beam steering direction (θ,ψ)= (45°,18°). File 4, ψ_s=18°, has been used.

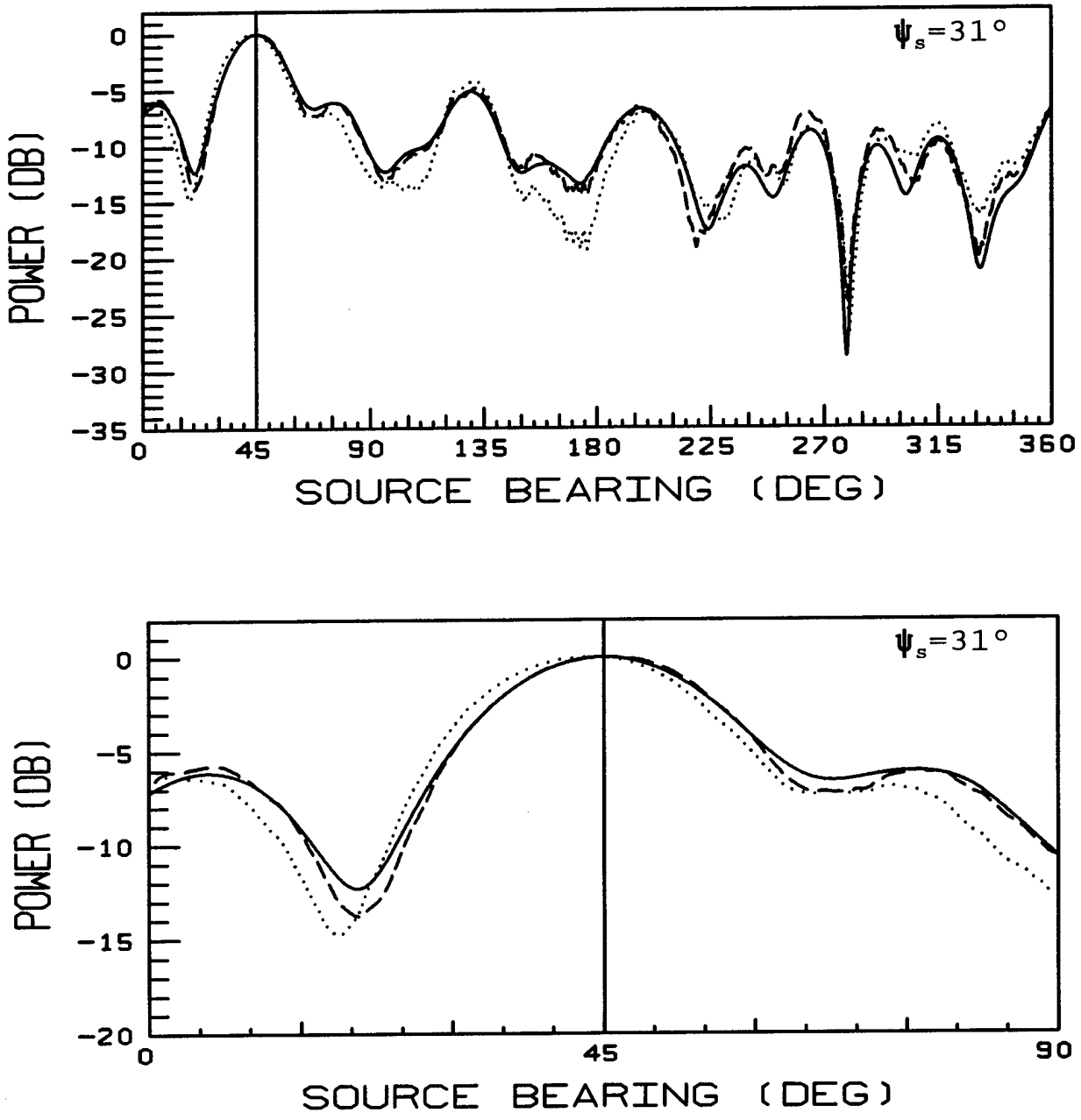

Fig. 16 The ideal (solid line), measured (dotted) and calibrated (broken) array beam patterns for beam steering direction (θ,ψ)= (45°,31°). File 5, ψ_s=31°, has been used.

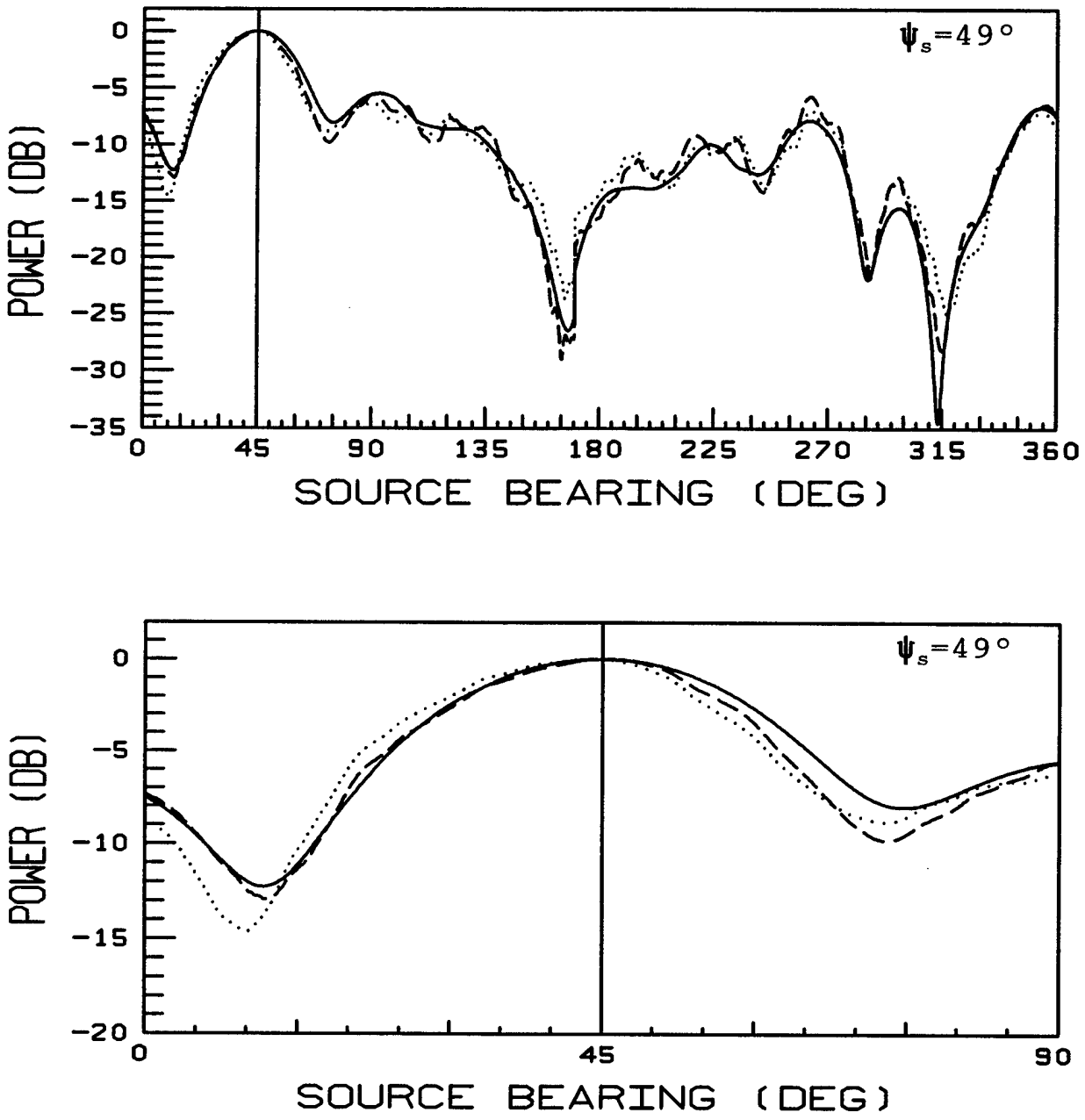

Fig. 17 The ideal (solid line), measured (dotted) and calibrated (broken) array beam patterns for beam steering direction (θ,ψ)= (45°,49°). File 6, ψ_s=49°, has been used.

do with the calibration experiment.

2. The measured beam patterns, in dotted lines, look similar to the ideal ones. There are biases in the positions of the main peaks, because they are not centred at θ_s=45°. These biases are easier to observe when the lower halves of the figures are examined.

   Further studies, to be presented later, show that the biases depend on source directions.

   Remark: The similarity indicates that the array snapshots can be used to estimate signal directions. The biases indicate that these estimates require corrections that depend on source directions.

3. The calibrated beam patterns, in broken lines, also look similar to the ideal ones. In Figs. 13 to 15, where $\psi_B=\psi_s\leq 18°$, the amplitudes in the three strongest lobes are closer to the ideal patterns than the measured ones. In Figs. 16 and 17, where ψ_B=31 and 49°, respectively, the identifiable effect of calibration is only a reduction of the biases in the main lobe positions.

   Remark: The calibration matrix calculated with File 2, where the source elevation is 11°, is effective for calibrating Files 1, 3 and 4. It is ineffective for Files 5 and 6.

4. In a separate study, not present here, the calibration matrix calculated with File 6 was used to calibrate File 6. The identifiable effect of this calibration was also a reduction of the bias in the main lobe position only.

   Remark: The calibration method cannot be used to calibrate File 6, because it has large measurement errors.

7.2 Effect on Direction Estimates

This study is restricted to the special case where there is only one signal in each array snapshot and that this signal is the direct signal from the transmitter. It uses the parametric target model fitting (PTMF) method [13-15], which is an HRDF method, to estimate the source bearing and elevation in the snapshots.

In the presentation of results, the error in a bearing estimates $\hat{\theta}$ is defined as

$$\epsilon(\hat{\theta}) = \hat{\theta} - \theta \ , \qquad (7.6)$$

where θ is the GPS bearing calculated with (3.2) and (3.3).

The errors in bearing estimates are plotted in point mode in Figs. 18 to 22. Those of the elevation estimates are in Figs. 23 to 27, respectively. Some notable observations are given below.

1. The estimates seem to fall on a smooth curve, although they are plotted in point modes.

   Remark: It appears that the SINRs in the preprocessed array snapshots are high and that the interfering environment did not change rapidly with source bearings.

2. Before calibration, the errors in bearing estimates depend strongly on the source bearings. Generally, they are positive in the 60° region and are negative in the 240° region. The calibration suppresses the dependence of errors on source bearings.

3. The calibration reduces the average magnitude of errors in bearing estimates. Many reductions are more than one degree in Figs. 18 to 20, where the source elevations are 18° or less.

4. There are strings of zero elevation estimates in Fig. 23, where the source elevation is 4.5°.

   Remark: The elevation estimates obtained from File 1 are not expected to be accurate. In this file, the antenna array aperture in the vertical direction is less than 0.2 wavelength for all source bearings. This aperture is too small to produce reliable elevation estimates.

   Remark: A separate study showed that, when an elevation estimate was zero, the PTMF method could usually produce a better fit to the data if it was allowed to use a value of $\cos(\hat{\psi})$ that was larger than unity. This $\cos(\hat{\psi})$ corresponded to a non-physical value of $\hat{\psi}$.

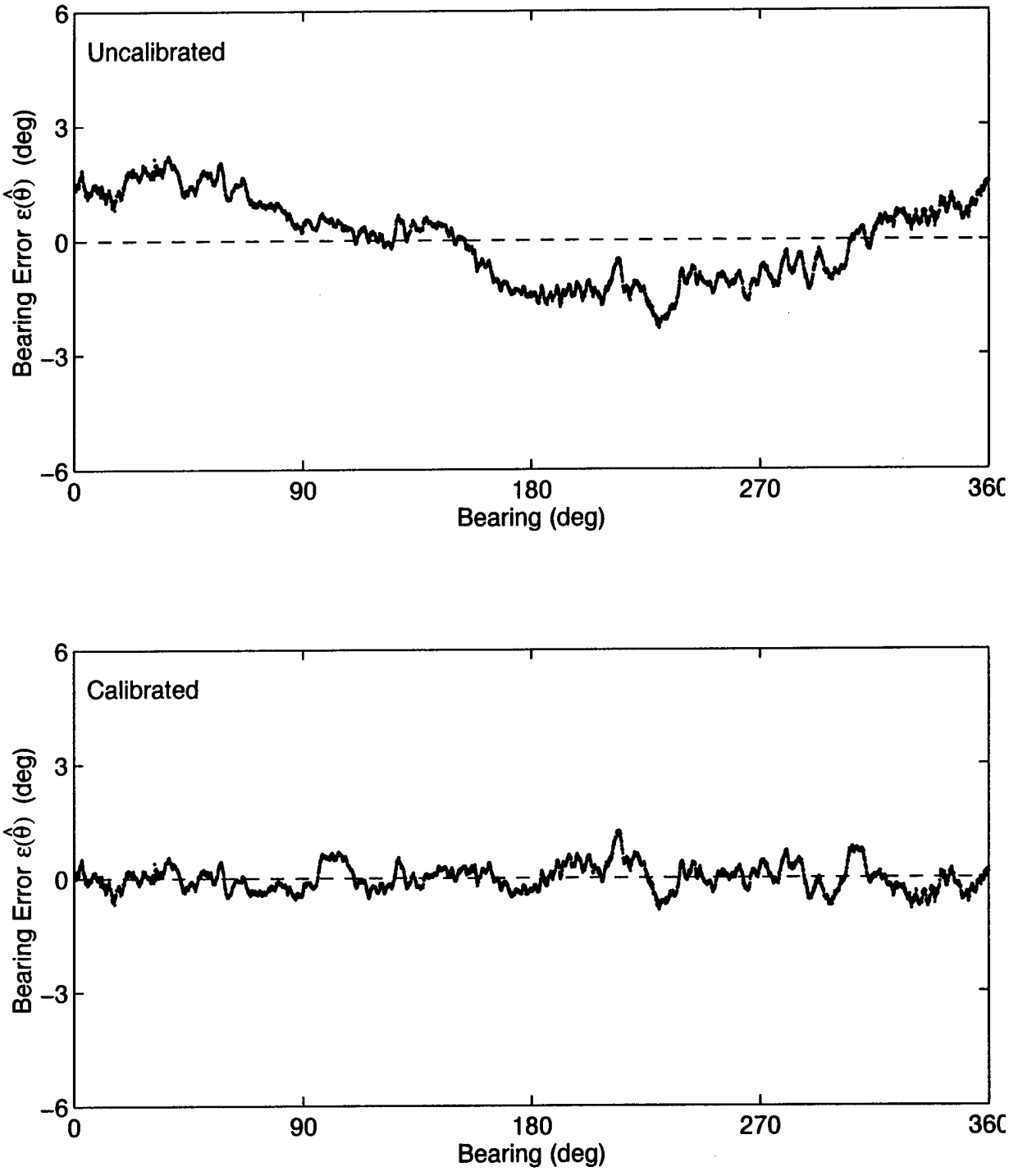

Figure 18. Errors in bearing estimates obtained with File 1. The upper figure is calculated with the uncalibrated data and the lower figure is calculated with the calibrated data.

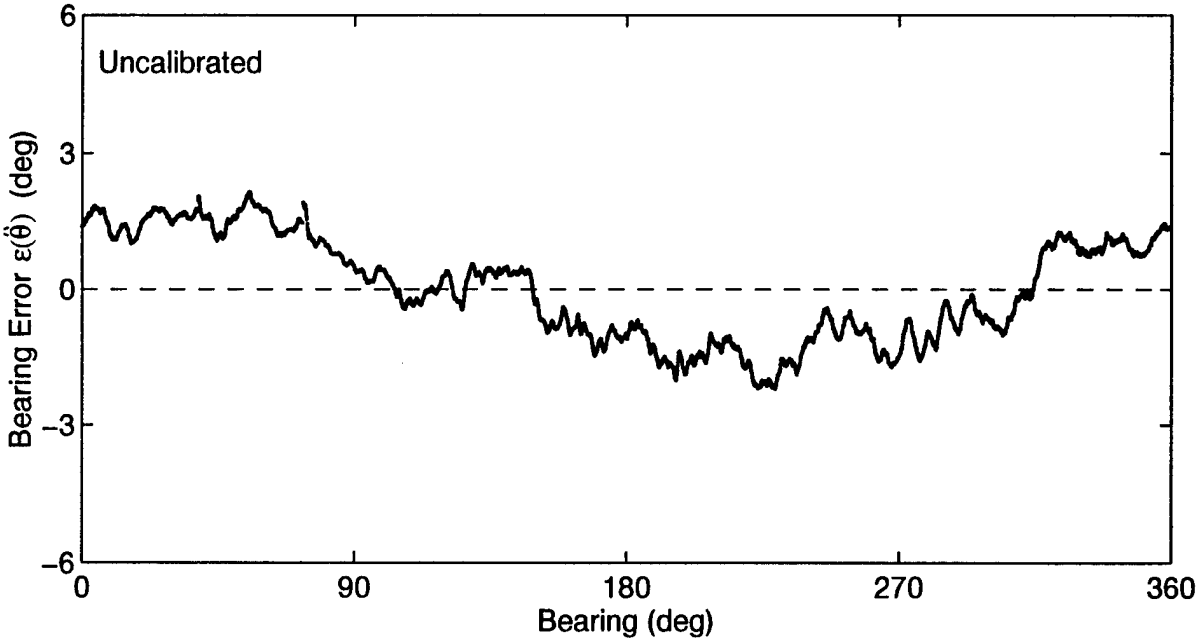

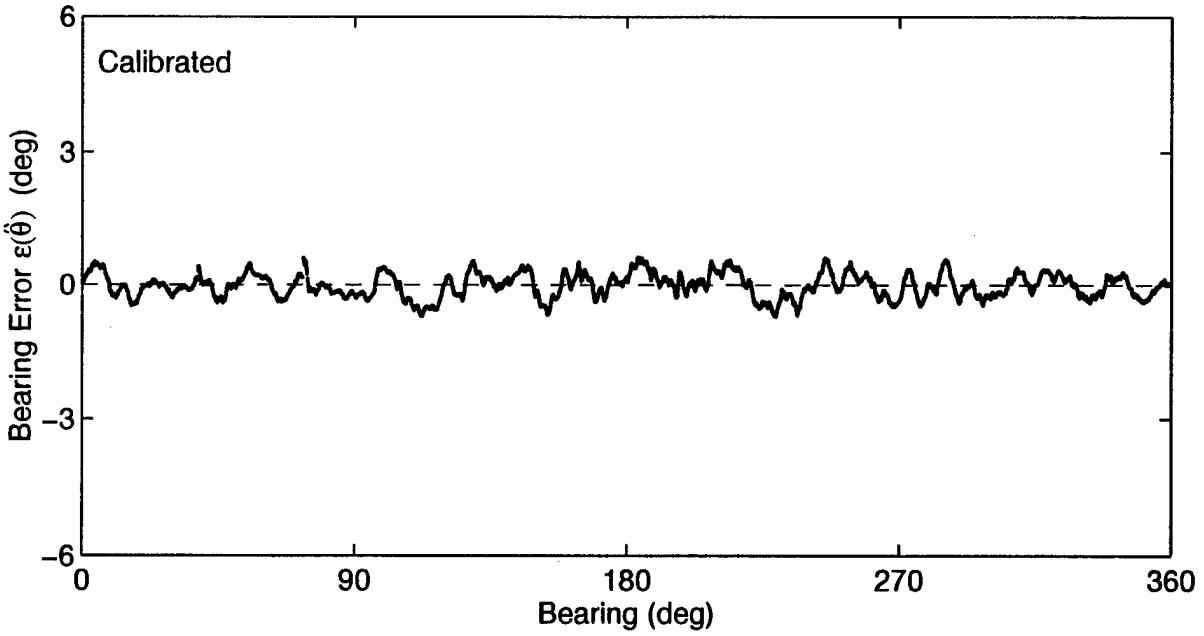

Figure 19. Errors in bearing estimates obtained with File 3.

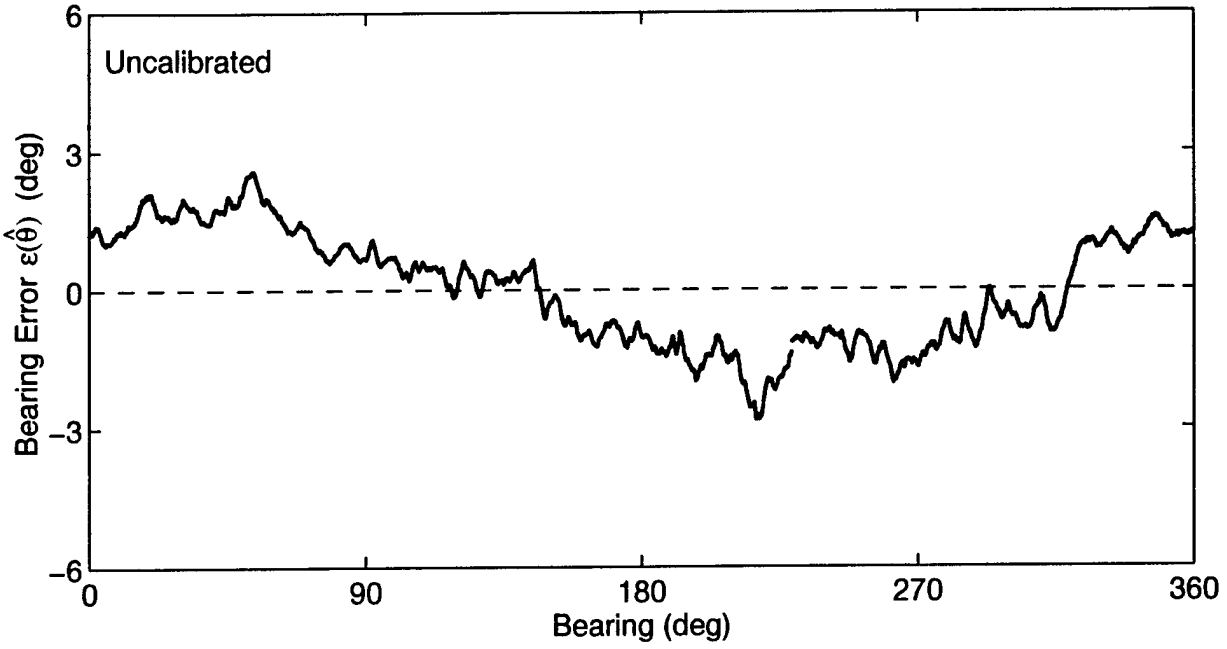

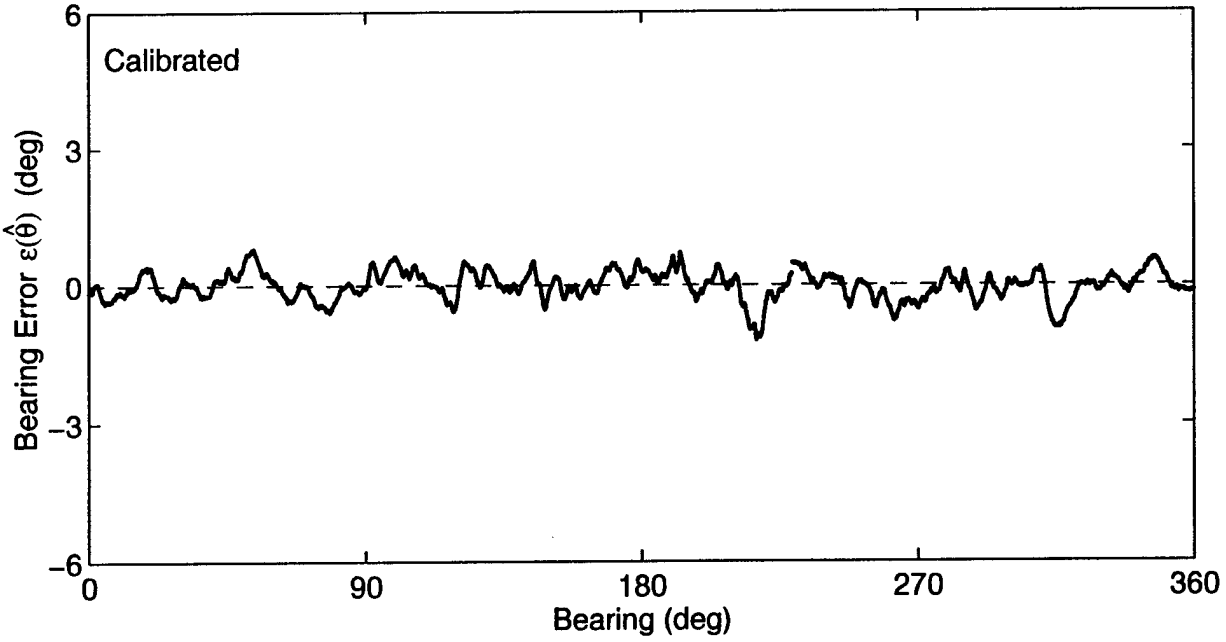

Figure 20. Errors in bearing estimates obtained with File 4.

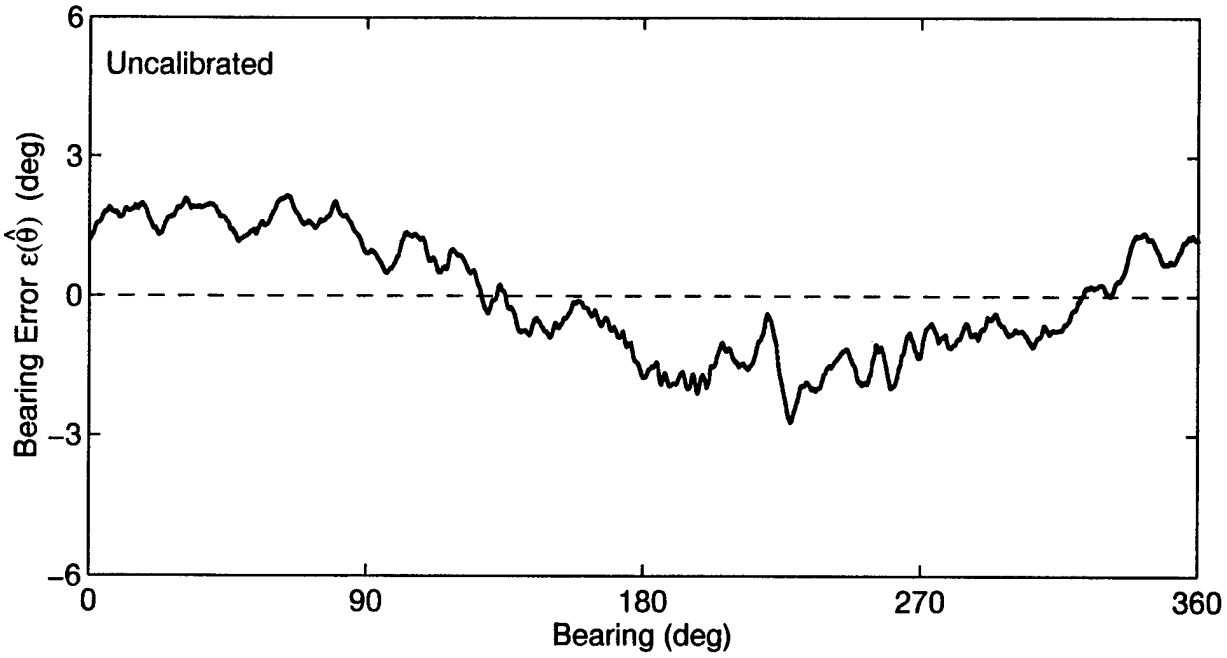

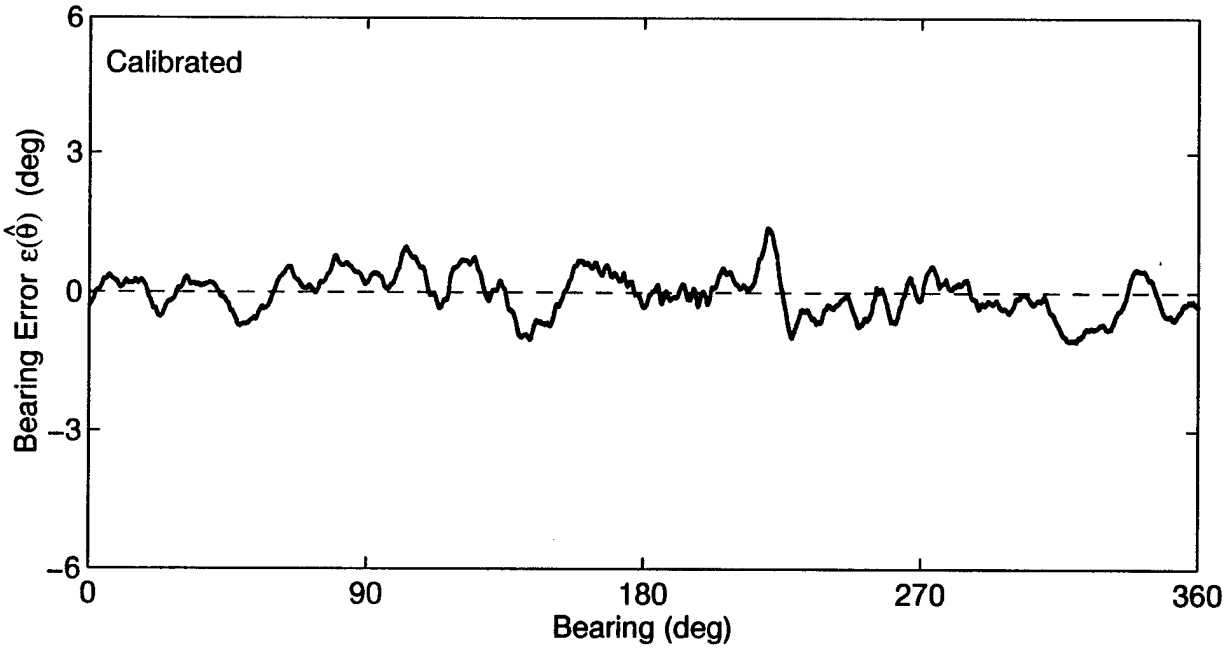

Figure 21. Errors in bearing estimates obtained with File 5.

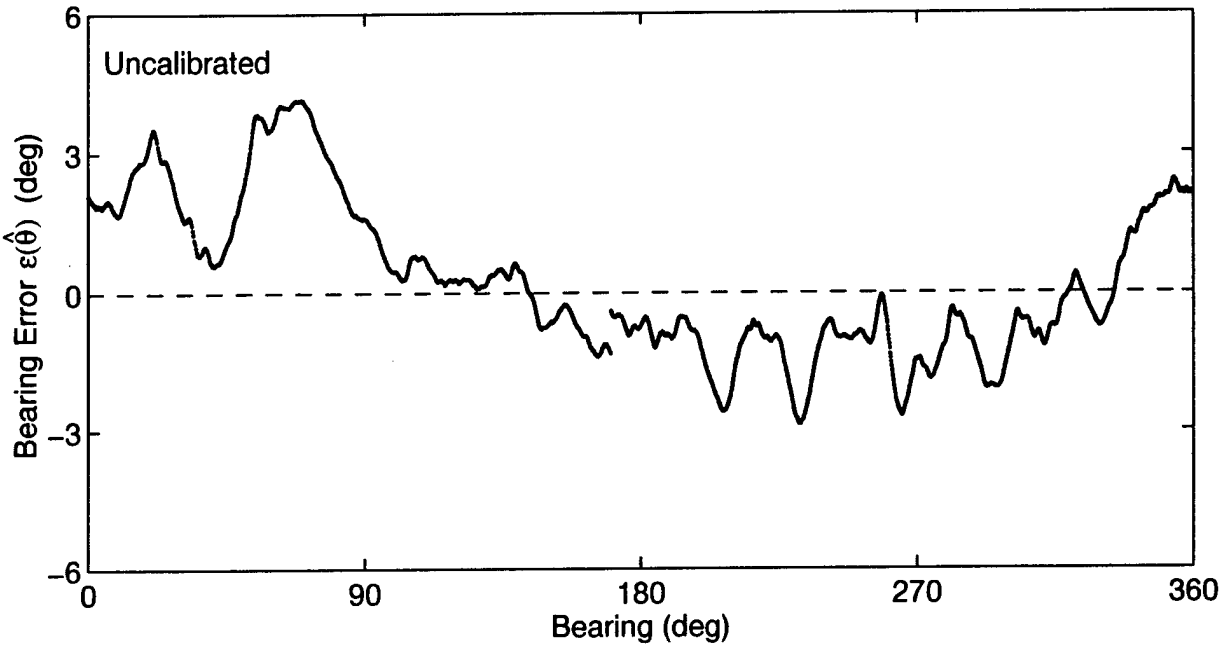

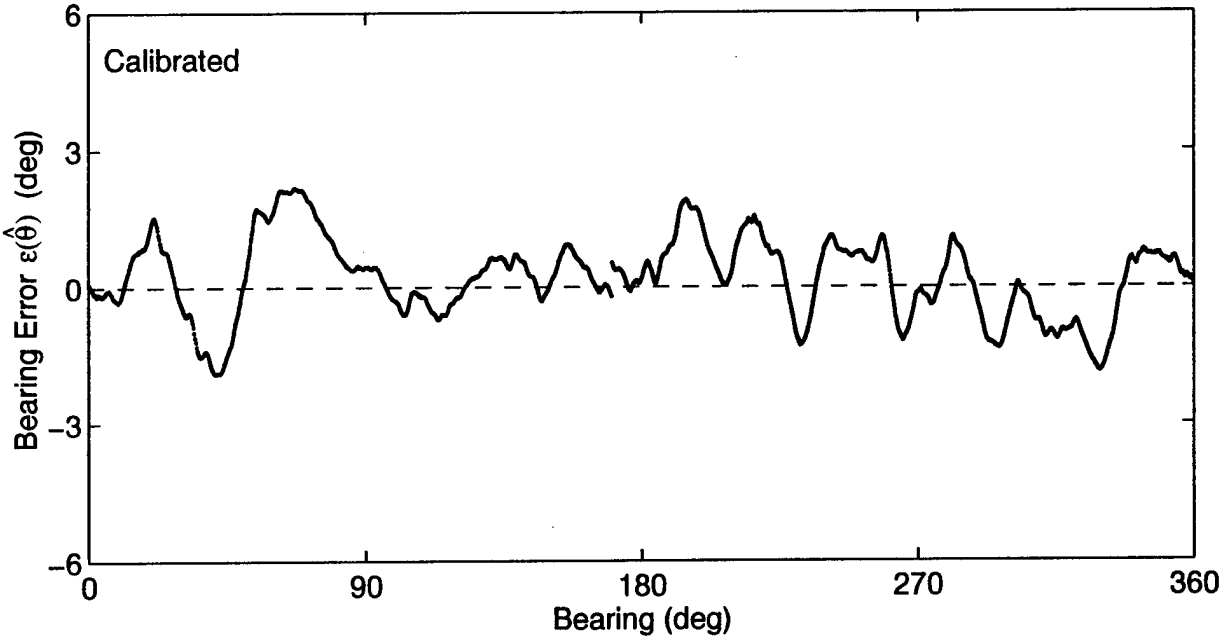

Figure 22. Errors in bearing estimates obtained with File 6.

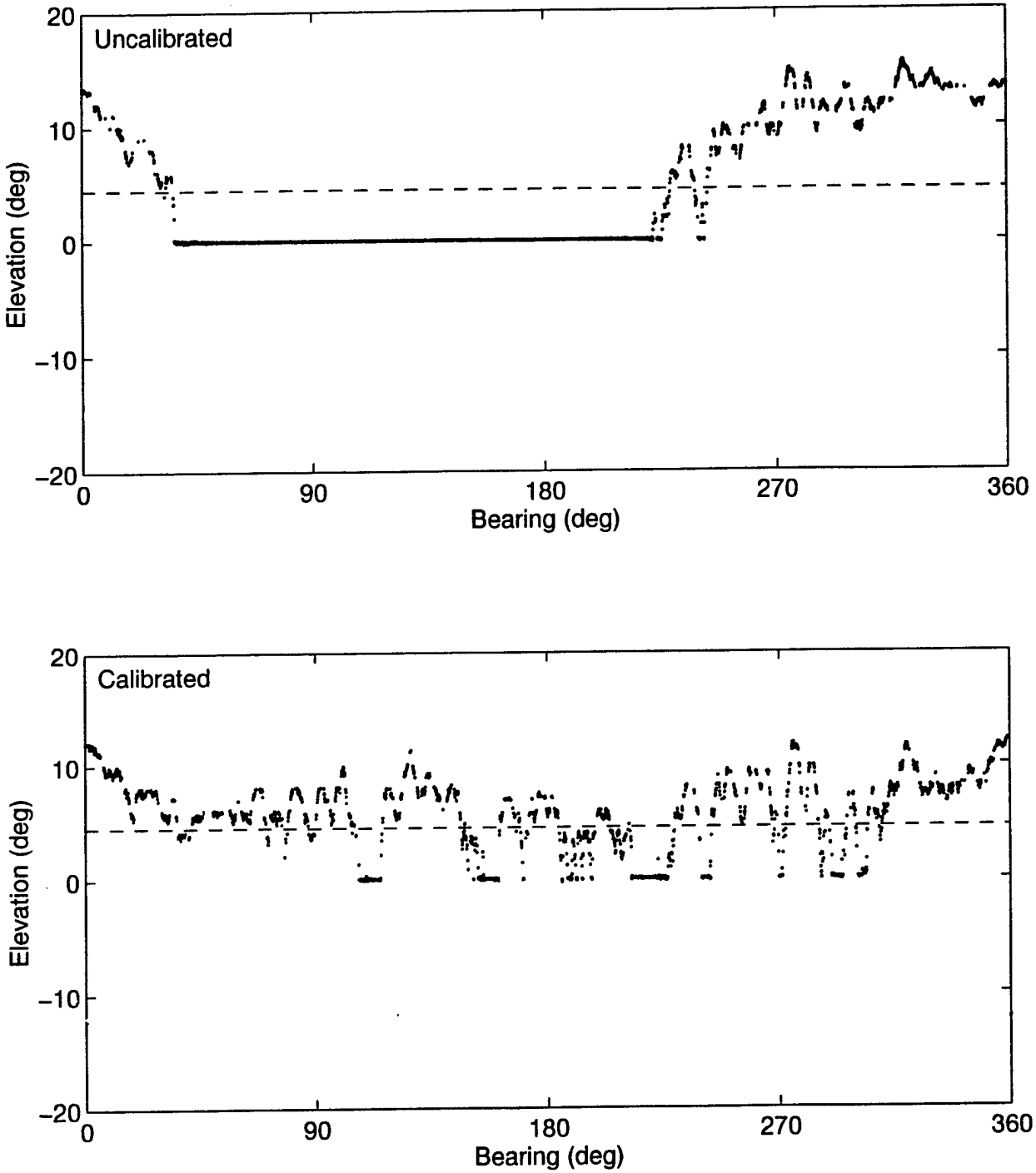

Figure 23. Elevation estimates obtained with File 1.

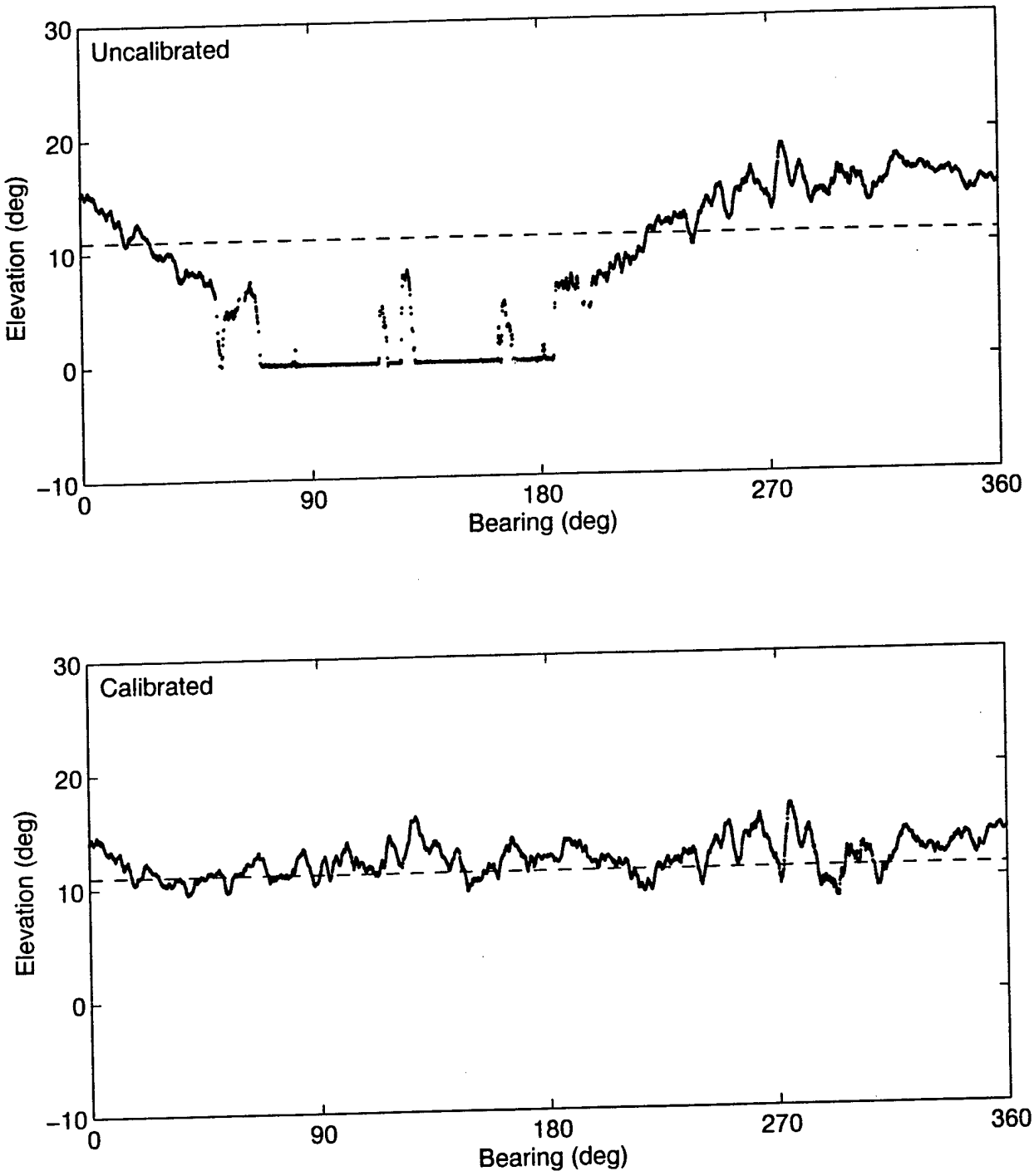

Figure 24. Elevation estimates obtained with File 3.

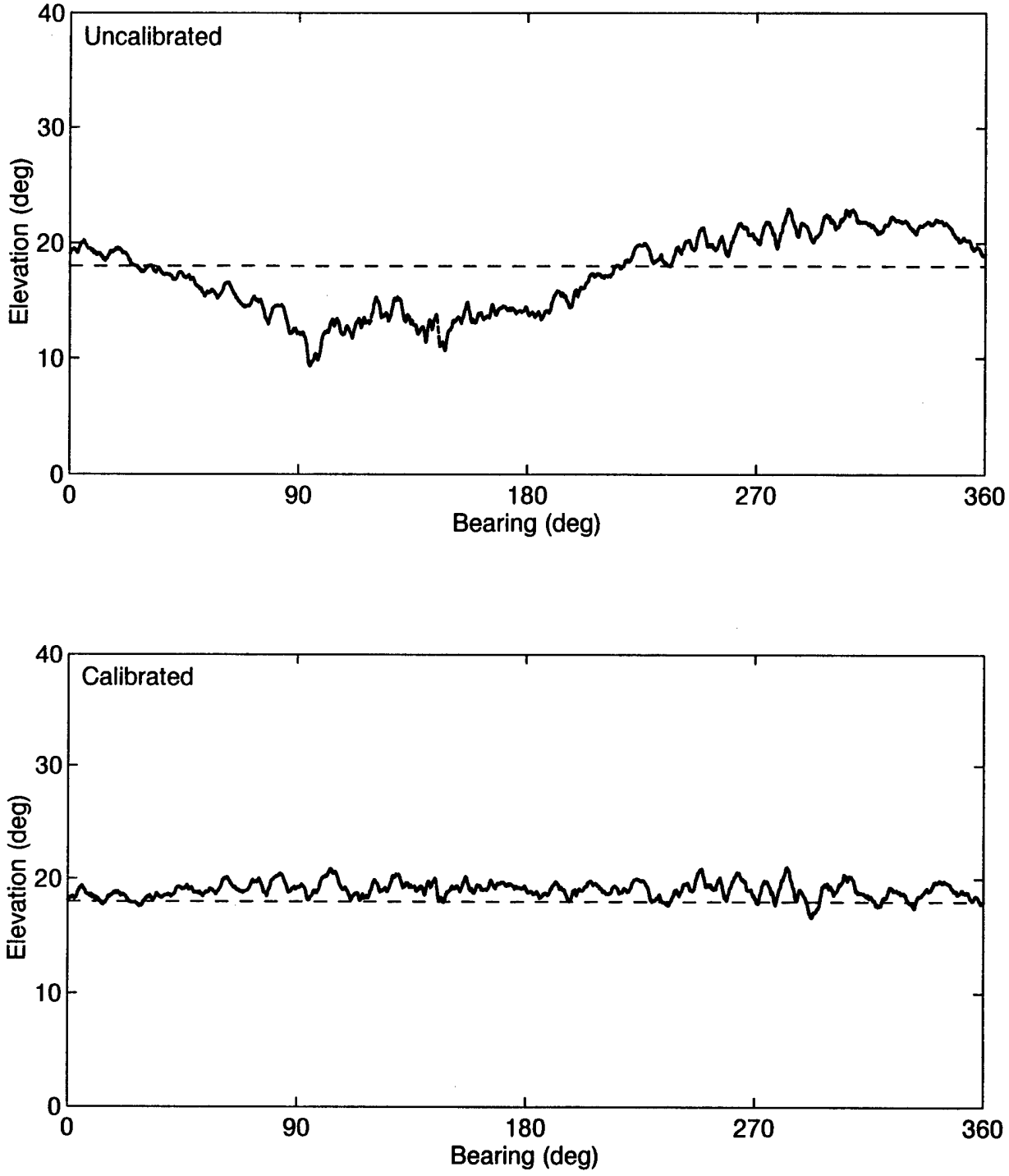

Figure 25. Elevation estimates obtained with File 4.

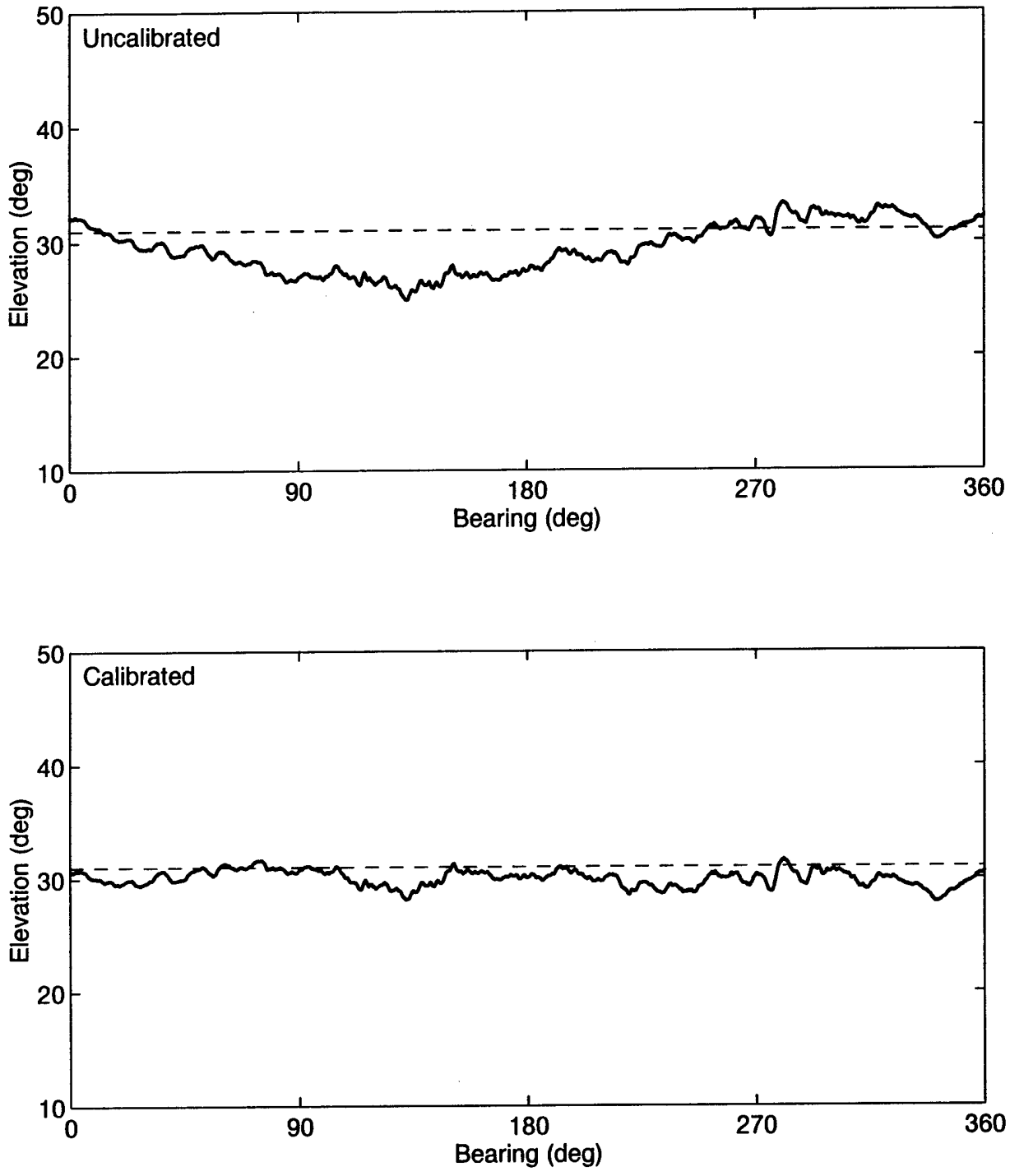

Figure 26. Elevation estimates obtained with File 5.

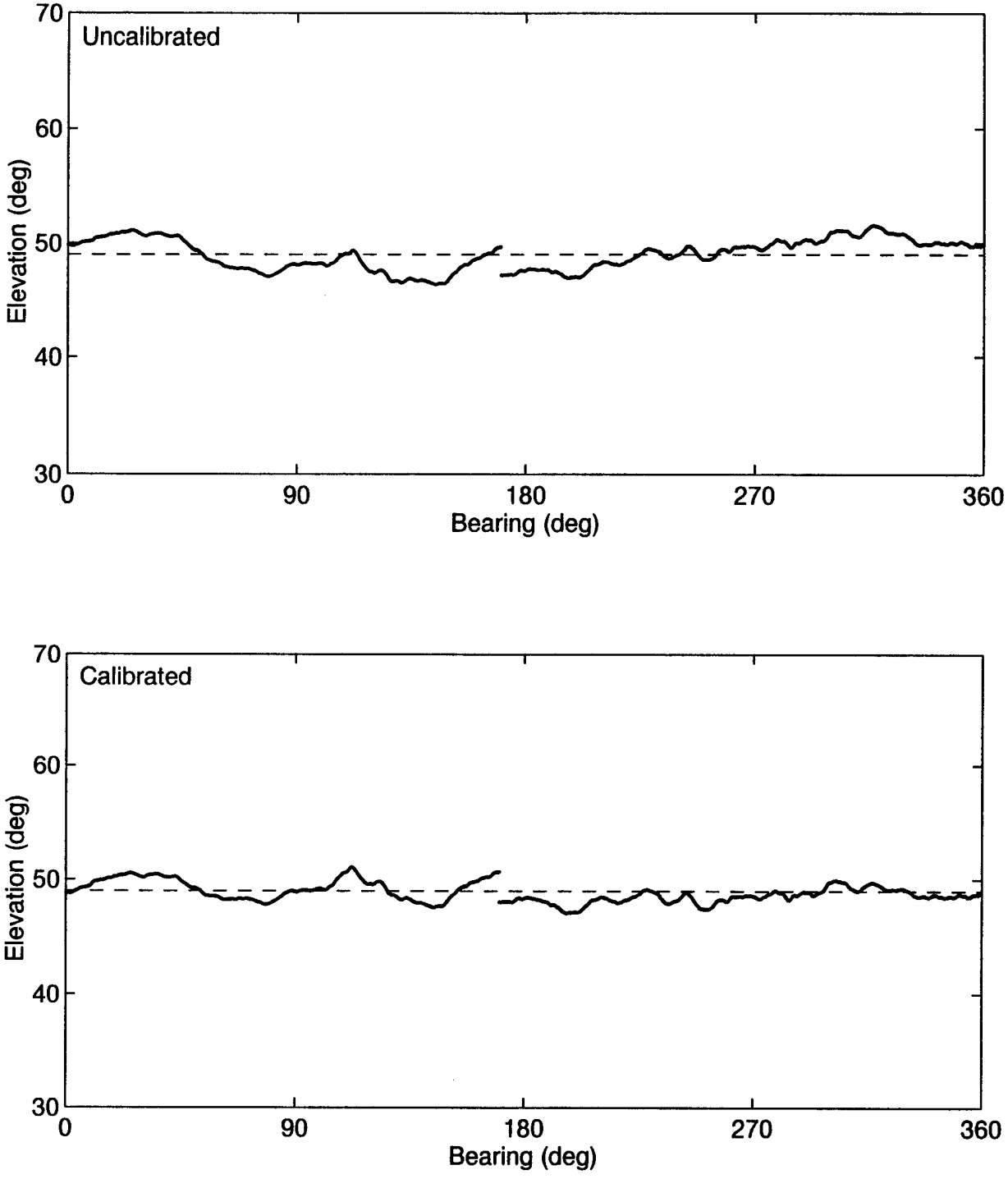

Figure 27. Elevation estimates obtained with File 6.

5. The upper halves of Figs. 24 to 26 show that the elevation estimates from Files 3 to 5, respectively, depend on the source bearings. In particular, they are below the nominal values in the neighbourhood of bearing θ_s=135° and above the nominal values in the neighbourhood of θ_s=315°. This dependence is not visible after calibration.

6. There are biases in the elevation estimates in Figs. 24 to 27. They depend on the files and are more noticeable in the lower halves of the figures.

   Remark: There are many possible reasons for these biases. They include flight path distortions, the deviation of transmitter altitudes from nominal altitudes, and the dependence of the Δ' in (3.2) on data files.

7. In both the upper and lower halves of Fig. 27, there are sudden drops of about 10° in elevation estimates at θ_s=172°.

   Remark: After preprocessing, the initial and final transmitter bearings in File 6 are 172° and 171.9°, respectively. From Fig. 8, the transmitter ranges are different for these two bearings. It is highly probable that the actual transmitter altitudes are also different.

7.3 Effect on Resolution of Signal Directions

This study compares the ability of the PTMF method to resolve the directions of two signal sources before and after calibration. It involves the construction of array snapshots with two signal sources present.

The study uses the five-step procedure described below. In Step 1, a section of 2K preprocessed array snapshots, denoted by $\{\mathbf{x}''_1, \mathbf{x}''_2, \mathbf{x}''_3, \cdots, \mathbf{x}''_{2K}\}$, is extracted from a specified file. This section is 60° wide in signal source bearing and the source bearing at the centre of the section is close to 30°. In Step 2, this section is separated into two groups given by $\{\mathbf{x}''_1, \mathbf{x}''_3, \mathbf{x}''_5, \cdots, \mathbf{x}''_{2K-1}\}$ and $\{\mathbf{x}''_{2K}, \mathbf{x}''_{2K-2}, \mathbf{x}''_{2K-4}, \cdots, \mathbf{x}''_2\}$. Because the ordering of the snapshots in the second group has been reversed, the source bearing increases from 0° to 60° in one group and decreases from 60° to 0° in the other. These two groups are then combined to produce a new set, denoted by $\{\mathbf{y}_1, \mathbf{y}_2, \mathbf{y}_3, \cdots, \mathbf{y}_K\}$, in which there are two signal

sources crossing each other near the 30° bearing. In Step 4, (7.8) is obtained from (5.14) by using $\mathbf{C}(2)$ instead of $\mathbf{C}$, $\mathbf{y}_k$ instead of $\mathbf{x}$, and $\mathbf{y}_k^c$ instead of $\mathbf{x}^c$. The details are given below:

Step 1.

Extracts a section of 2K snapshots with source bearings between 0° and 60° from a specified file. Identify the snapshots by $\{\mathbf{x}'_1, \mathbf{x}'_2, \mathbf{x}'_3, \cdots, \mathbf{x}'_{2K}\}$.

Step 2.

Construct a set of K new snapshots $\{\mathbf{y}_1, \mathbf{y}_2, \mathbf{y}_3, \cdots, \mathbf{y}_K\}$ as

$$\mathbf{y}_k = \mathbf{x}'_{2k-1} + \mathbf{x}'_{2K+2-2k} , \qquad k=1,2,3,\ldots,K . \tag{7.7}$$

Step 3.

Use the PTMF method to estimate two signal directions from each snapshot in $\{\mathbf{y}_1, \mathbf{y}_2, \mathbf{y}_3, \cdots, \mathbf{y}_K\}$. Denote the estimates obtained from $\mathbf{y}_k$ by $\{\hat{\theta}_{k1}, \hat{\psi}_{k1}\}$ and $\{\hat{\theta}_{k2}, \hat{\psi}_{k2}\}$.

Step 4.

Construct a set of K calibrated snapshots $\{\mathbf{y}_1^c, \mathbf{y}_2^c, \mathbf{y}_3^c, \cdots, \mathbf{y}_K^c\}$ as

$$\mathbf{y}_k^c = \mathbf{C}(2)\mathbf{y}_k , \qquad k=1,2,\cdots,K . \tag{7.8}$$

Step 5.

Use the PTMF method to estimate two signal directions from each snapshot in $\{\mathbf{y}_1^c, \mathbf{y}_2^c, \mathbf{y}_3^c, \cdots, \mathbf{y}_K^c\}$. Denote them by $\{\hat{\theta}_{k1}^c, \hat{\psi}_{k1}^c\}$ and $\{\hat{\theta}_{k2}^c, \hat{\psi}_{k2}^c\}$.

The value of K is 300 for Files 1 and 3 to 5, and 170 for File 6. It is smaller for File 6, because this file is smaller and the array snapshots are spaced farther apart in bearing.

Figs. 28 to 32 contain the bearing estimates $\hat{\theta}_{k1}$, $\hat{\theta}_{k2}$, $\hat{\theta}_{k1}^c$, and $\hat{\theta}_{k2}^c$ obtained. These estimates are plotted in point mode. Each figure has two solid lines. They are nominal source tracks calculated with (3.2) and

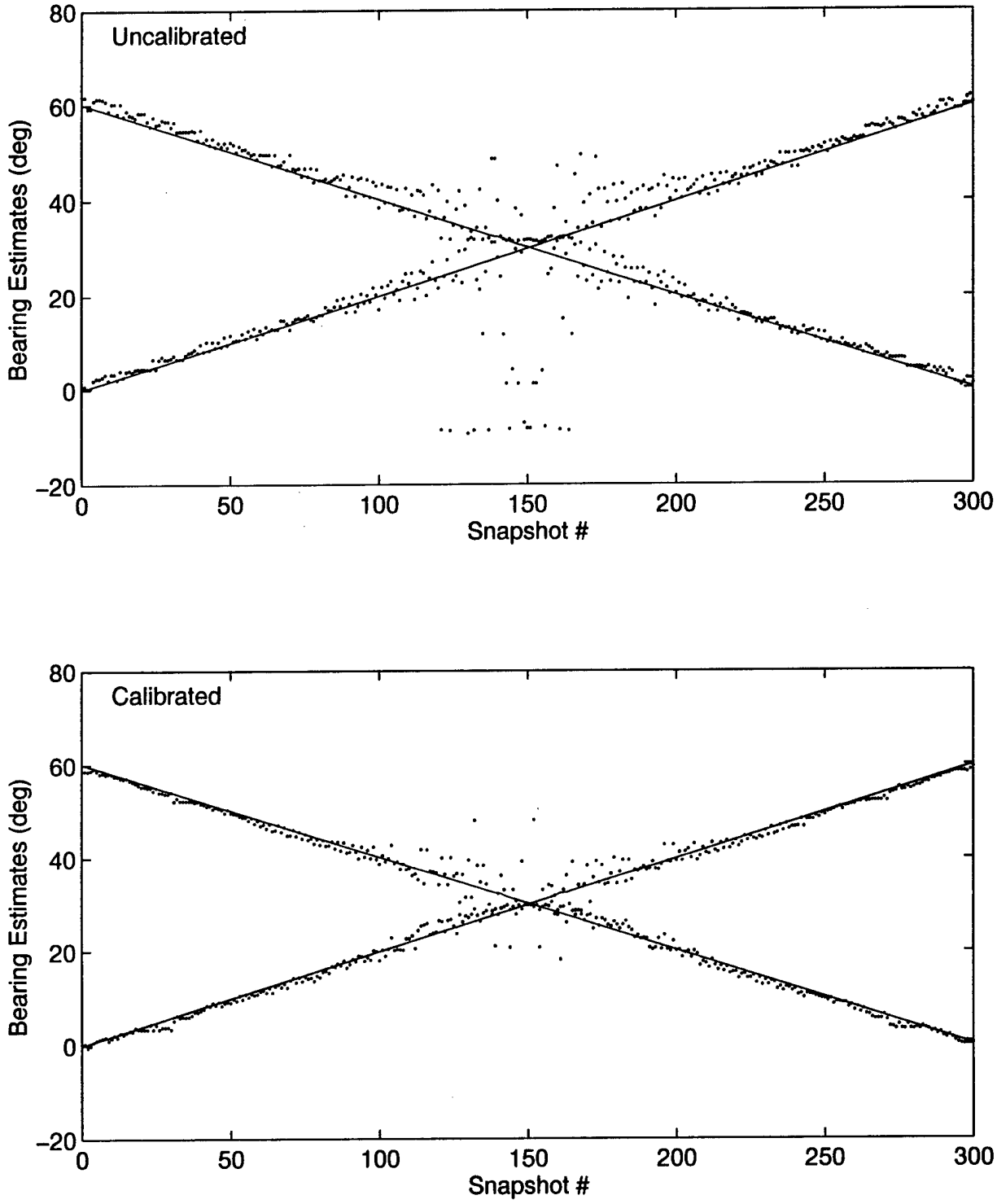

Figure 28. Bearing estimates (points) calculated with File 1. The solid lines represent the nominal source tracks.

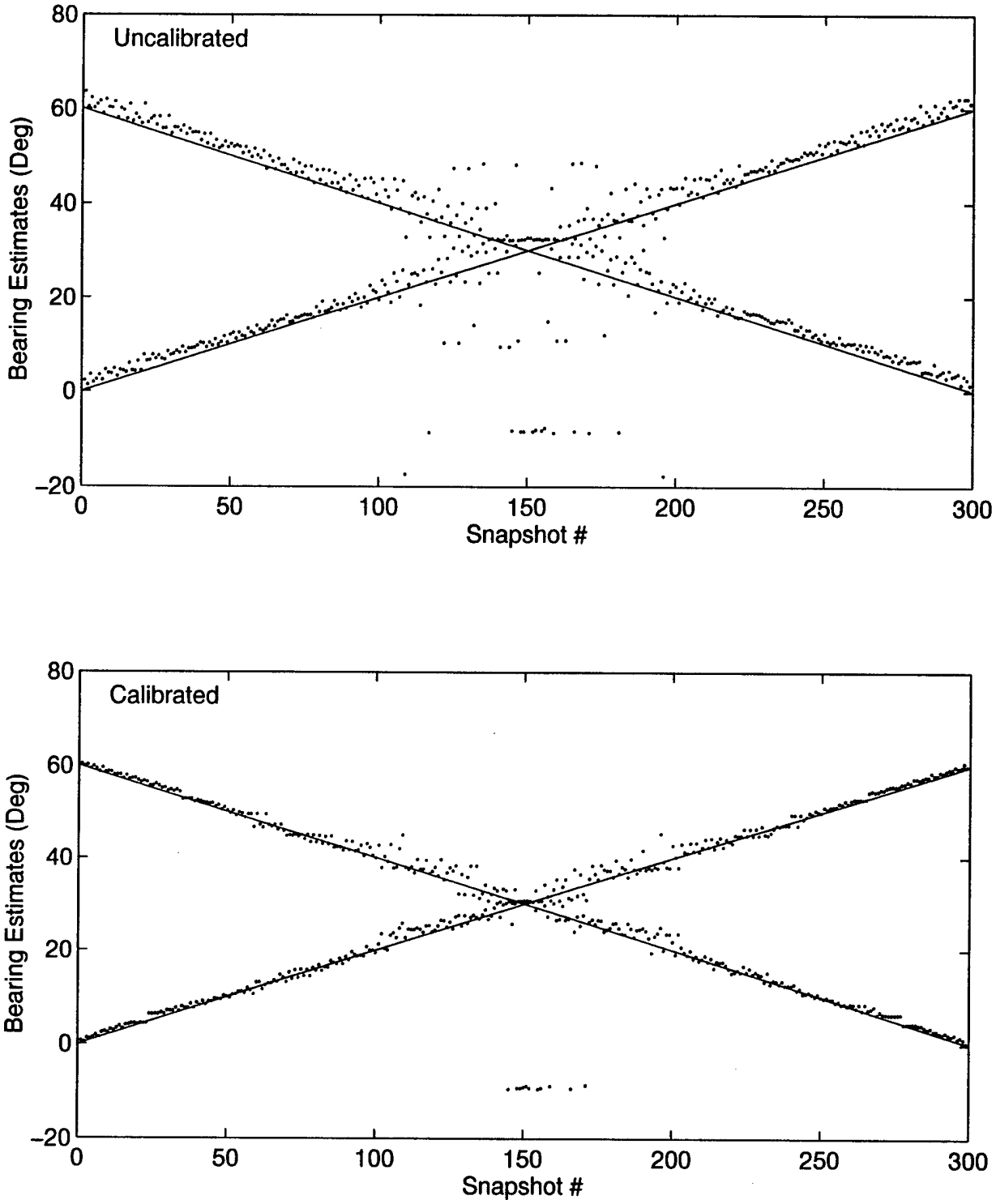

Figure 29. Bearing estimates (points) calculated with File 3.

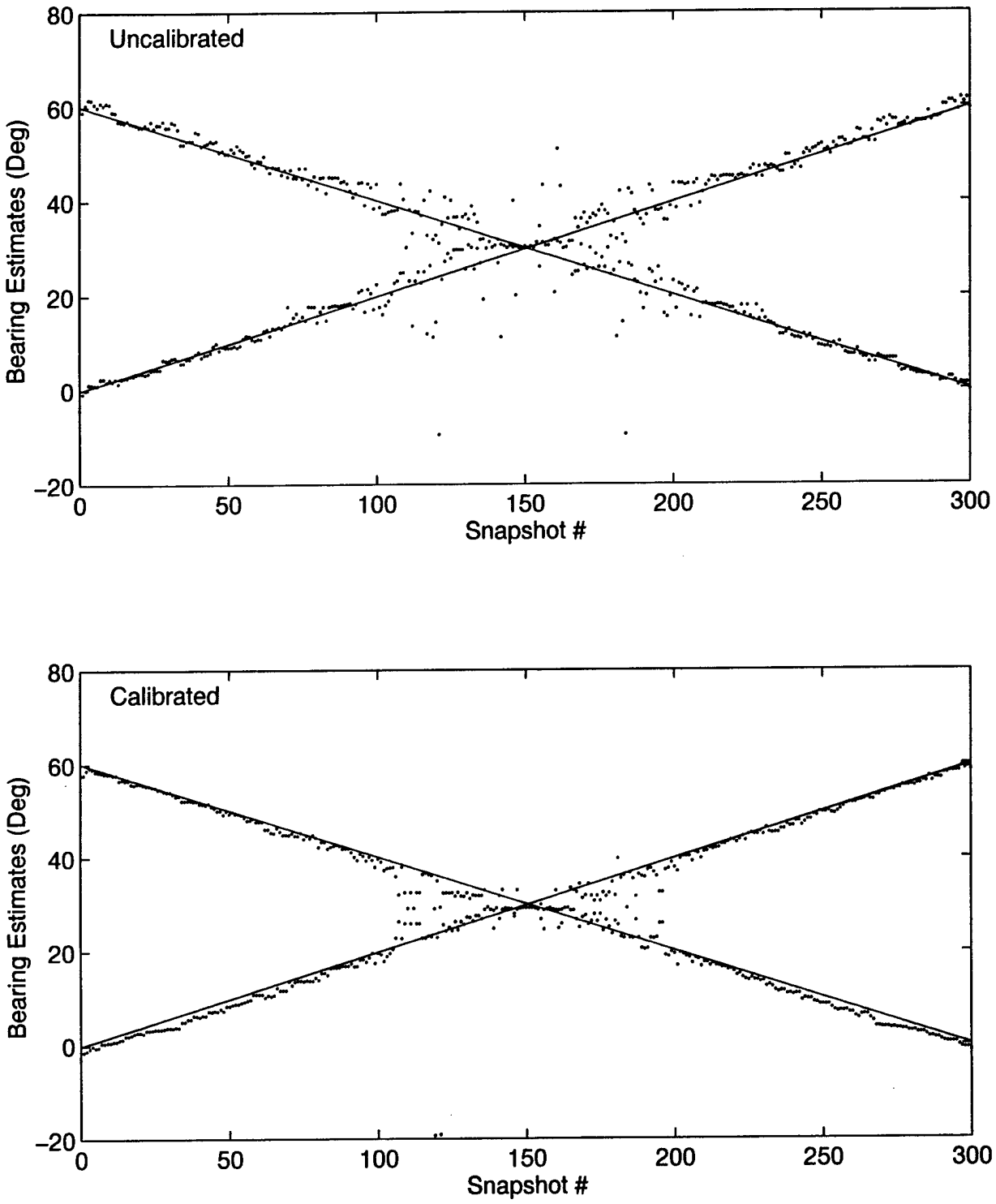

Figure 30. Bearing estimates (points) calculated with File 4.

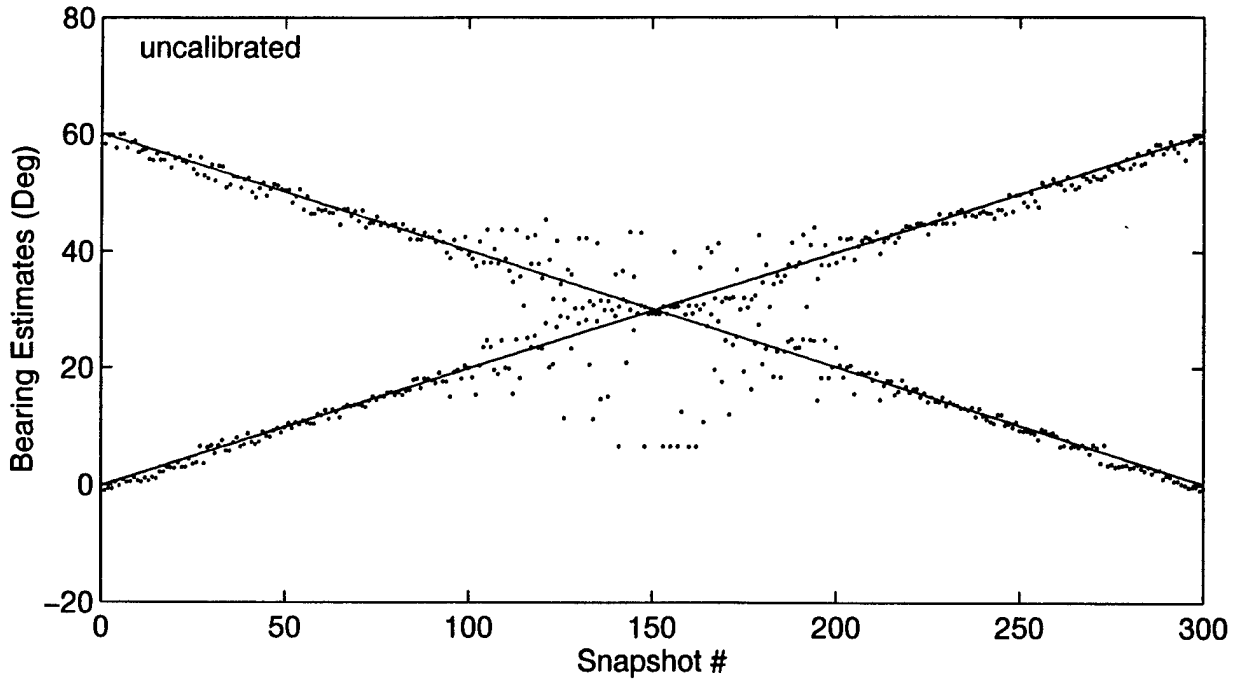

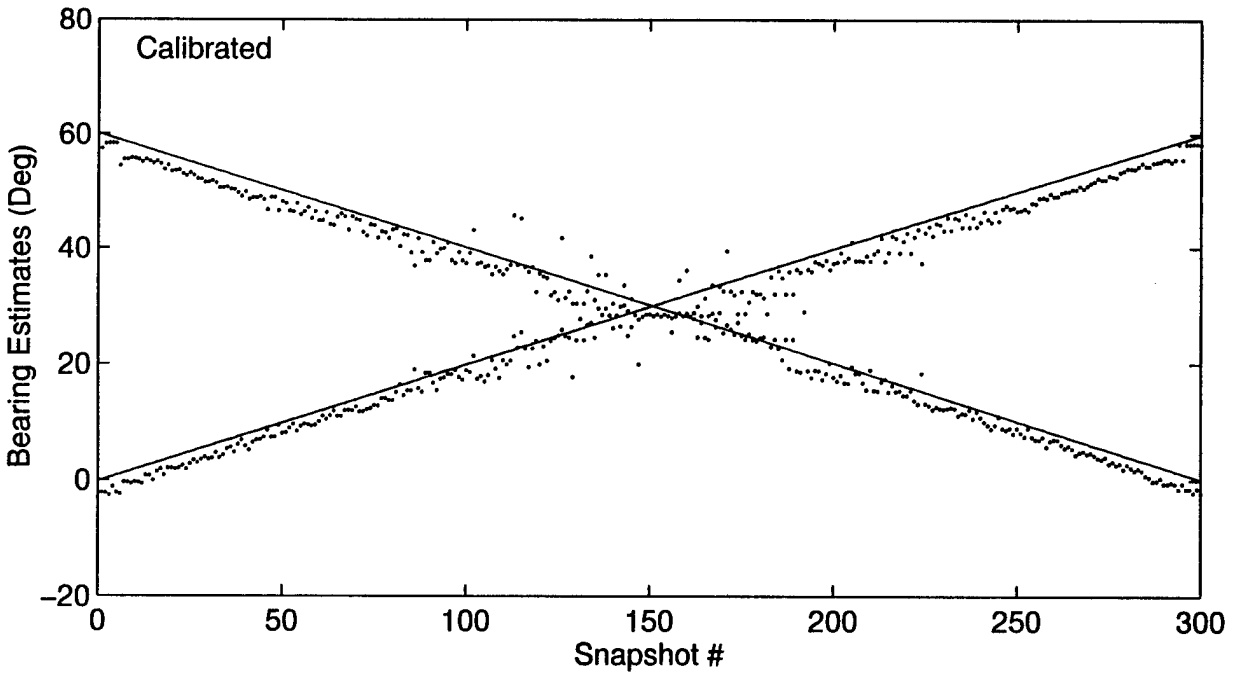

Figure 31. Bearing estimates (points) calculated with File 5.

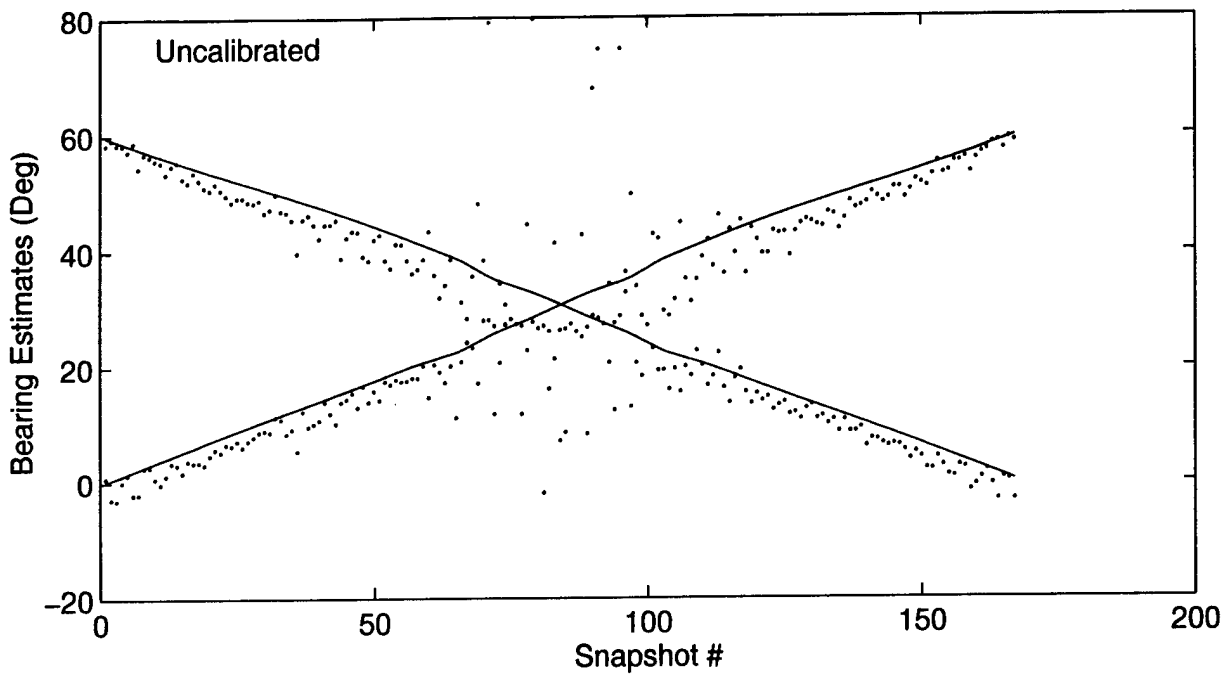

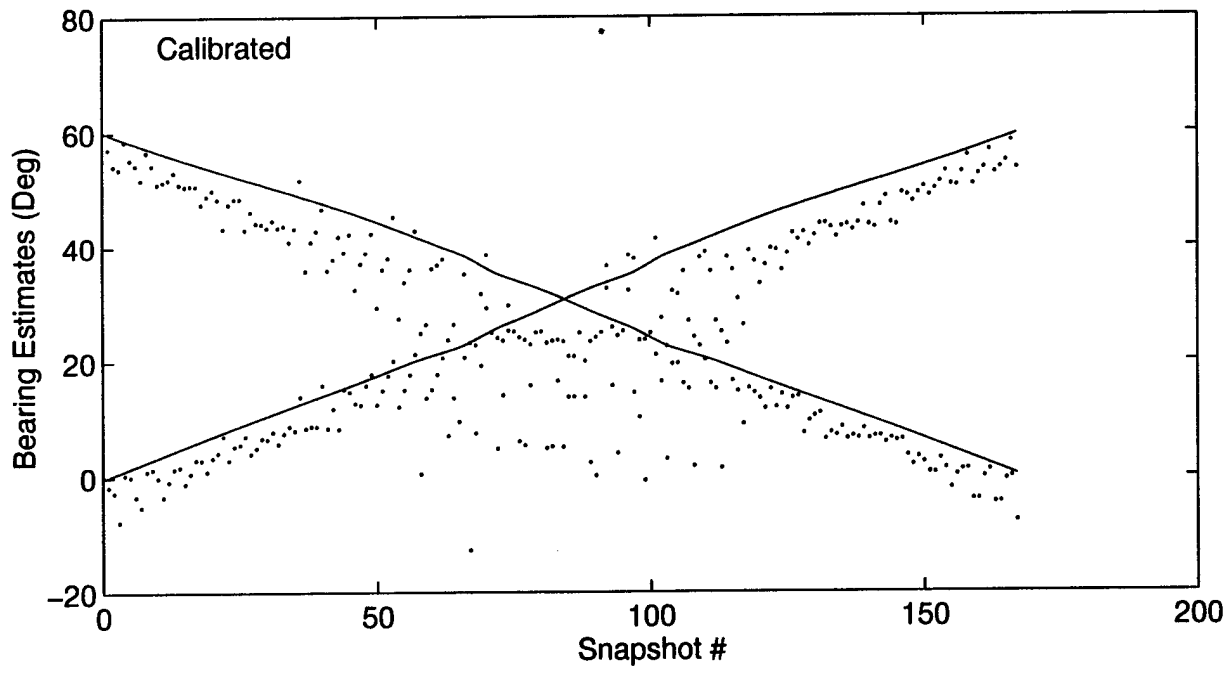

Figure 32. Bearing estimates (points) calculated with File 6. The true signal tracks are given by the solid lines.

(3.3). One is the source track in $\{\mathbf{x}''_1, \mathbf{x}''_3, \mathbf{x}''_5, \cdots, \mathbf{x}''_{2K-1}\}$. The other is the source track in $\{\mathbf{x}''_{2K}, \mathbf{x}''_{2K-2}, \mathbf{x}''_{2K-4}, \cdots, \mathbf{x}''_2\}$. There are several notable observations:

1. In each figure, the bearing estimates seem to cluster around two apparent tracks that intersect near the 30° bearing.

2. The apparent tracks deviate from the nominal tracks given by the solid lines. In particular, all are above the nominal tracks before calibration.

   Remark: The deviations are related to the errors in bearing estimates in Figs. 18 to 22. Before calibration, the bearing estimates are larger than the nominal bearings in the bearing range 0° to 60°. This agrees with the observation that the apparent tracks are above the nominal tracks.

3. The scattering of the points about the apparent tracks is generally larger if the angular separation of the true signal bearings is smaller.

   Remark: This property is expected, because it is more difficult to resolve two signal directions that are closer together in directions. More difficulty in resolution leads to larger errors in the estimates.

4. The calibration reduces the scattering of the bearing estimates about the apparent tracks.

8.0 CONCLUSIONS

The authors have carried out a second analysis of the 5.1 MHz calibration data measured with a high-frequency (HF) antenna array at Leitrim. This analysis used the second antenna array calibration method [1] developed by Eric Hung at DREO. It was part of a task to develop a calibration method for the HF antenna arrays in the Canadian Forces Supplementary Radio Systems (CFSRS) modernization project. These arrays are used for detecting long-range HF signals and estimating their directions.

The following observations are based on the analysis of data files generated with signal source elevations 31° or lower:

1. The calibration method reduces the deviation of the antenna beam patterns from the ideal patterns;

2. The method increases the accuracy of direction estimates and suppresses the dependence of errors in bearing estimates on source bearings; and

3. The method increases the ability of an HRDF method to resolve signal directions.

4. The method is superior to the first antenna array calibration method. In particular, the direction estimates are more accurate and the ability of an HRDF method to resolve signal directions is better.

It is not possible to remark on the results obtained with calibration data generated with signal source elevations higher than 31°. The results are very encouraging. However, these data files have large errors that cannot be suppressed.

ACKNOWLEDGEMENTS

The authors would like to thank Petrie Telecommunications Ltd. for planning and conducting the pattern measurement system and the aircraft flight measurements. They also want to thank Paul Soble and Richard Larose of the Canadian Security Establishment for their assistance in making an antenna array available for the measurements and providing the digital recording.

REFERENCES

1. Eric K.L. Hung, "Computation of the Coupling Matrix Among the Elements of an Array Antenna," 1994 International Conference on Radar (Radar 94), pp. 703-706, Paris, May 1994.

2. A. Paulraj and T. Kailath, "Direction of Arrival Estimation by Eigenstructure Methods with Unknown Sensor Gain and Phase," ICASSP 1985, Tampa, U.S.A., pp. 640-643, March 1985.

3. B. Friedlander and A. J. Weiss, "Eigenstructure Methods for Direction Finding with Sensor Gain and Phase Uncertainties," ICASSP 1988, New York, U.S.A., pp. 2681-2684, April 1988.

4. A. J. Weiss and B. Friedlander, "Eigenstructure Methods for Direction Finding with Sensor Gain and Phase Uncertainties," Circuits and Systems and Signal Processing, vol. 9, No. 3, pp. 271-300, 1990.

5. G. C. Brown, J. H. McClellan and E. J. Holder, "A Phased Array Calibration Technique using Eigenstructure Methods," IEEE 1990 International Radar Conference, Arlington, U.S.A., pp. 304-307, May 1990.

6. G. C. Brown, J. H. McClellan and E. J. Holder, "Eigenstructure Approach for Array Processing and Calibration with General Phase and Gain Perturbations," ICASSP 91, Toronto, Canada, pp. 3037-3040, May 1991.

7. J. Pierre and M. Kaveh, "Experimental Performance of Calibration and Direction-Finding Algorithms," ICASSP 91, Toronto, Canada, pp. 1365-1368, May 1991.

8. Eric K.L. Hung, "Estimation of Array Element Gains and Phases in the Presence of Specular Multipath," 1994 International Conference on Radar (RADAR 94), pp. 162-166, Paris, May 1994

9. C.M.S. See, "Sensor Array Calibration in the Presence of Mutual Coupling and Unknown Sensor Gains and Phases," Electronics Letters,

Vol 30, pp. 373-374, March 1994.

10. C.M.S. See, "Method for Array Calibration in High-Resolution Sensor Array Processing," IEE Proceedings on Radar, Sonar and Navigation, Vol. 142, pp. 90-96, June 1995.

11. M. C. Dogan and J. M. Mendel, "Applications of Cumulants to Array Processing - Part I: Aperture Extension and Array Calibration," IEEE Transactions on Signal Processing, Vol. 43, pp. 1200-1216, May 1995.

12. Xinping Huang and Eric K.L. Hung, "Analysis of the Calibration Data Measured with a High-Frequency Antenna Array," DREO Report No. 1289, Defence Research Establishment Ottawa, Ottawa, Ontario. August, 1996.

13. Eric K.L. Hung, "A Critical Study of a Self-Calibrating Direction-Finding Method for Arrays," IEEE Transactions on Signal Processing, Vol. 42, pp. 471-474, February 1994.

14. R.W. Jenkins, "Antenna Amplitude and Phase Pattern Measurements using an Aircraft-Towed Transmitter," CRC Report No. 95-003, Communications Research Centre, Ottawa, Ontario, September 1995.

15. U. Nickel, "Radar Target Parameter Estimation with Array Antennas," in Chapter 3, Radar Array Processing ed. by S. Haykin, J. Litva and T.J. Shepherd (Springer-Verlag, New York, 1992).

UNCLASSIFIED

SECURITY CLASSIFICATION OF FORM
(highest classification of Title, Abstract, Keywords)

DOCUMENT CONTROL DATA

(Security classification of title, body of abstract and indexing annotation must be entered when the overall document is classified)

1. ORIGINATOR (the name and address of the organization preparing the document. Organizations for whom the document was prepared, e.g. Establishment sponsoring a contractor's report, or tasking agency, are entered in section 8.)

Department of National Defence
Defence Research Establishment Ottawa
Shirleys Bay, Ottawa, Ontario K1A 0K2

2. SECURITY CLASSIFICATION (overall security classification of the document including special warning terms if applicable)

UNCLASSIFIED

3. TITLE (the complete document title as indicated on the title page. Its classification should be indicated by the appropriate abbreviation (S,C or U) in parentheses after the title.)

Analysis of the HF data measured at Leitrim, using a matrix calibration method developed at DREO (U)

4. AUTHORS (Last name, first name, middle initial)

Eric K.L. Hung (DREO)

Zhijiang Hu (Telexis Corp.)

5. DATE OF PUBLICATION (month and year of publication of document)

6a. NO. OF PAGES (total containing information. Include Annexes, Appendices, etc.)

70

6b. NO. OF REFS (total cited in document)

15

7. DESCRIPTIVE NOTES (the category of the document, e.g. technical report, technical note or memorandum. If appropriate, enter the type of report, e.g. interim, progress, summary, annual or final. Give the inclusive dates when a specific reporting period is covered.)

Technical Report

8. SPONSORING ACTIVITY (the name of the department project office or laboratory sponsoring the research and development. Include the address.)

Department of National Defence, Defence Research Establishment Ottawa
Shirleys Bay, Ottawa, Ontario K1A 0K2

9a. PROJECT OR GRANT NO. (if appropriate, the applicable research and development project or grant number under which the document was written. Please specify whether project or grant)

05B09

9b. CONTRACT NO. (if appropriate, the applicable number under which the document was written)

W7714-4-0188

10a. ORIGINATOR'S DOCUMENT NUMBER (the official document number by which the document is identified by the originating activity. This number must be unique to this document.)

DREO REPORT 1319

10b. OTHER DOCUMENT NOS. (Any other numbers which may be assigned this document either by the originator or by the sponsor)

11. DOCUMENT AVAILABILITY (any limitations on further dissemination of the document, other than those imposed by security classification)

(X) Unlimited distribution
( ) Distribution limited to defence departments and defence contractors; further distribution only as approved
( ) Distribution limited to defence departments and Canadian defence contractors; further distribution only as approved
( ) Distribution limited to government departments and agencies; further distribution only as approved
( ) Distribution limited to defence departments; further distribution only as approved
( ) Other (please specify):

12. DOCUMENT ANNOUNCEMENT (any limitation to the bibliographic announcement of this document. This will normally correspond to the Document Availabilty (11). However, where further distribution (beyond the audience specified in 11) is possible, a wider announcement audience may be selected.)

UNCLASSIFIED

SECURITY CLASSIFICATION OF FORM

13. ABSTRACT (a brief and factual summary of the document. It may also appear elsewhere in the body of the document itself. It is highly desirable that the abstract of classified documents be unclassified. Each paragraph of the abstract shall begin with an indication of the security classification of the information in the paragraph (unless the document itself is unclassified) represented as (S), (C), or (U). It is not necessary to include here abstracts in both offical languages unless the text is bilingual).

This is the second report on the analysis of the calibration data taken with a high frequency (HF) antenna array and a signal source towed behind a small aircraft. The analysis described in this report uses the second of two array calibration methods developed by E.K.L. Hung at DREO; the previous report uses the first method. This work is part of a bigger task to develop a calibration method for the HF antenna arrays in the Canadian Forces Supplementary Radio Systems (CFSRS) modernization project.

The calibration method used in this report is superior to the method used in the previous report. The results derived from the calibration data generated with source elevations 31° or lower show that it reduces the deviation of the array beam patterns from the ideal ones, reduces the errors in signal direction estimates, and increases the ability of a high-resolution direction-finding method to resolve signal directions.

14. KEYWORDS, DESCRIPTORS or IDENTIFIERS (technically meaningful terms or short phrases that characterize a document and could be helpful in cataloguing the document. They should be selected so that no security classification is required. Identifiers, such as equipment model designation, trade name, military project code name, geographic location may also be included. If possible keywords should be selected from a published thesaurus. e.g. Thesaurus of Engineering and Scientific Terms (TEST) and that thesaurus-identified. If it is not possible to select indexing terms which are Unclassified, the classification of each should be indicated as with the title.)

Antenna Array
Calibration
High Frequency
Direction Finding